



저작자표시-비영리-변경금지 2.0 대한민국

이용자는 아래의 조건을 따르는 경우에 한하여 자유롭게

- 이 저작물을 복제, 배포, 전송, 전시, 공연 및 방송할 수 있습니다.

다음과 같은 조건을 따라야 합니다:



저작자표시. 귀하는 원저작자를 표시하여야 합니다.



비영리. 귀하는 이 저작물을 영리 목적으로 이용할 수 없습니다.



변경금지. 귀하는 이 저작물을 개작, 변형 또는 가공할 수 없습니다.

- 귀하는, 이 저작물의 재이용이나 배포의 경우, 이 저작물에 적용된 이용허락조건을 명확하게 나타내어야 합니다.
- 저작권자로부터 별도의 허가를 받으면 이러한 조건들은 적용되지 않습니다.

저작권법에 따른 이용자의 권리는 위의 내용에 의하여 영향을 받지 않습니다.

이것은 [이용허락규약\(Legal Code\)](#)을 이해하기 쉽게 요약한 것입니다.

[Disclaimer](#)

공학박사 학위논문

Effects of Human Body on UWB Channel in Indoor Environments

실내 환경에서 초광대역 채널에 미치는 인체의
영향

2015년 8월

서울대학교 대학원

전기컴퓨터공학부

김 영 훈

공학박사 학위논문

Effects of Human Body on UWB Channel in Indoor Environments

실내 환경에서 초광대역 채널에 미치는 인체의
영향

2015년 8월

서울대학교 대학원

전기컴퓨터공학부

김 영 훈

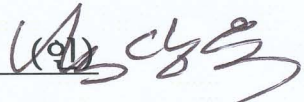


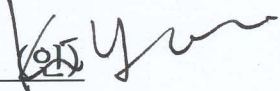
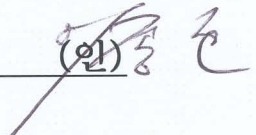
EFFECTS OF HUMAN BODY ON
UWB CHANNEL IN INDOOR
ENVIRONMENTS

지도 교수 김 성 철

이 논문을 공학박사 학위논문으로 제출함
2015년 8월

서울대학교 대학원
전기, 컴퓨터공학부
김 영 훈

김영훈의 박사 학위논문을 인준함
2015년 7월

위원장	남 상 욱	(인) 
부위원장	김 성 철	(인) 
위원	박 세 응	(인) 
위원	김 영 록	(인) 
위원	이 중 호	(인) 

Abstract

EFFECTS OF HUMAN BODY ON UWB CHANNEL IN INDOOR ENVIRONMENTS

Young-Hoon Kim

Department of Electrical Engineering and Computer Science

The Graduate School

Seoul National University

In this dissertation, the effects of human body on Ultra Wideband (UWB) channel in indoor environments are represented. Unlike previous communication system, UWB system has a large bandwidth. This leads to interference to the other communication systems in the same frequency bands. This feature makes UWB system deployable in line-of-sight (LOS) and slightly cluttered non-line-of-sight (NLOS) environment in which the signal undergoes less attenuation. In these environments, the UWB channel largely depends on surroundings of a transmitter (Tx) and receiver (Rx) antennas. In indoor environments, a human body is a major factor that changes channel characteristics. This dissertation dealt with the effect of human body on the UWB channel in indoor environments.

First, this dissertation addresses UWB channel variation depending on the number of people in indoor LOS environments. To assess variation of UWB channels, four environments which have different room sizes and wall structures are considered. During measurements, people did not move around, but were just sitting on their chair with small motion if necessary. Because the UWB system operates in a wide bandwidth compared to previous communication systems, it is necessary to understand the frequency correlation characteristics of UWB channels. We found the correlation coefficients between two frequency tones with an interval of 10MHz are smaller than about 0.5. In the dissertation, we deal with a distance-dependent path-loss model, a frequency-dependent path-loss model, and time dispersion parameters. To provide a general channel model, we obtained the linear regression model with population density for each parameter.

Next, the dissertation considered a situation where either LOS path is not blocked or slightly blocked by human bodies as a Rx is shifted by small-scale (1λ) distance while a Tx is fixed. In this situation, we measure the small-scale amplitude statistics in the absence and presence of human bodies and propose a statistical model of the small-scale fading distribution. From the measurement data, we found the best fitted channel model among several typical theoretical distribution models such as Lognormal, Nakagami, and Weibull distributions, showing good agreement with the empirical channel data.

In the last part of dissertation, we dealt with the performance analysis of impulse radio (IR) UWB system based on the proposed small-scale fading distribution and also compare the performance with the existing channel model.

Due to the fine time resolution of UWB system, the system mainly uses a rake receiver which consists of a number of correlators that are sampled at the delays related to specific number of multipath components. The dissertation considers two types of rake receiver, selective combining (SC) and partial combining (PC) rake receiver. The standard channel model, IEEE 802.15.4a, shows the best bit-error-rate (BER) performance. But this model does not include the effect of human body. When the effect of human body is included on 802.15.4a model, the BER performance is deteriorated.

Keywords: UWB Channel modeling, Human body, IR-UWB, Rake receiver, BER performance,

Student Number: 2007-20949

Contents

Chapter 1 Introduction.....	1
1.1 UWB system.....	1
1.2 UWB channel standard model.....	2
1.2.1 IEEE 802.15.3a.....	2
1.2.2 IEEE 802.15.4a.....	2
1.3 Motivation.....	3
1.4 Dissertation Outline.....	5
Chapter 2 Modeling of UWB channel with Population density in indoor LOS Environments.....	6
2.1 Introduction.....	6
2.2 Measurement Methodology	8
2.2.1 Measurement System.....	8
2.2.2 Measurement Scenario.....	9
2.3 Frequency Correlation Coefficient of the Measured Channel Gains	12
2.4 Path-Loss Characteristics.....	15
2.4.1 Empirical distance-dependent path-loss model.....	15

2.4.2 Empirical frequency-dependent path-loss model.....	18
2.5 Time-Dispersion Parameters.....	22
2.6 Conclusion.....	26
Chapter 3 Human body Affected Small-Scale Fading for indoor UWB channel.....	27
3.1 Introduction.....	27
3.2 Measurement Campaign.....	28
3.2.1 Measurement System.....	28
3.2.2 Measurement Scenario.....	28
3.3 Statistical Modeling of Small-Scale Fading	35
3.4 Small-Scale Fading Distribution by Body.....	37
3.5 Conclusions.....	48
Chapter 4 Performance Analysis of Rake receiver in IR-UWB system.....	49
4.1 Introduction.....	49
4.2 UWB Rake receiver.....	51
4.2.1 UWB Rake receiver structure... ..	51
4.2.2 Rake Receiver Type... ..	54

4.3 Channel models.....	56
4.3.1 801.15.4a UWB channel model	56
4.3.2 People Shadowing Effect on UWB Channels.....	58
4.4 BER performance analysis.....	60
4.5 Conclusion.....	66
Bibliography.....	67
Abstract in Korean.....	70

List of Tables

Table 1.1	Typical environment and ranges for UWB applications.....	1
Table 2.1	Size, Area, Max. No. of people, and Main features.....	10
Table 2.2	Empirical Distance-dependent Path-loss Parameters.....	16
Table 2.3	Empirical Frequency-dependent Path-loss Parameters.....	20
Table 3.1	Size and Main features of all environments.....	29
Table 3.2	Passing Rate For The Scenarios In The Absence of Human Body.....	39
Table 3.3	Passing Rate For The Scenarios In The Presence of Human Body.....	39
Table 3.4	The parameters of the exponential fit for λ	45
Table 3.5	The parameters of the Lognormal fit for κ	47
Table 4.1	Main Difference of Channel Models.....	61

List of Figures

Figure 2.1	Block diagram of the measurement system.....	8
Figure 2.2	Floor plans for no people and 10 people in B environment.....	13
Figure 2.3	Correlation Coefficient with Δf	11
Figure 2.4	Distance-dependent path-loss model and its regression model...	13
Figure 2.5	Methods for obtaining frequency-dependent path-loss model...	17
Figure 2.6	Frequency-dependent path-loss model and its regression model.....	21
Figure 2.7	Mean excess delay and RMS delay spread.....	24
Figure 2.8	Normalized power delay profile.....	25
Figure 3.1	Floor plans for all environments.....	34
Figure 3.2	Typical the normalized power delay profile of a sample data file.....	37
Figure 3.3	CDFs of passing rate of Weibull distribution in the presence of human bodies.....	40
Figure 3.4	CDFs of the empirical small-scale fading amplitude fitted with Weibull distribution in the absence of human bodies and in the presence of human bodies.....	41

Figure 3.5	λ with delay time and its regression model fitted with the exponential function.....	44
Figure 3.6	CDF of κ and their regression model fitted with Lognormal distribution in the presence of human bodies.....	46
Figure 4.1	A Rake receiver structure.....	53
Figure 4.2	Principle of (a) SC-Rake and (b) PC-Rake receiver.....	55
Figure 4.3	Computation of blocking angular range and Power attenuation when a person moves along a path perpendicular to LOS.....	59
Figure 4.4	BER with the number of fingers for (a) SC-Rake receiver and (b) PC-Rake receiver.....	63
Figure 4.5	BER performance of a 10-finger SC-Rake receiver and PC-Rake receiver.....	65

Chapter 1. Introduction

1.1 UWB system

Ultra-Wide-Band (UWB) systems are commonly defined as the systems that have either more than 20% relative bandwidth or more than a 500 MHz absolute bandwidth. It is well known that UWB systems have many advantages [1]: 1) Accurate position location and ranging, due to the fine time resolution, 2) no significant multipath fading due to fine time resolution, 3) multiple access due to wide transmission bandwidth, 4) possibility of extremely high data rates, 5) covert communications due to low transmission power operation, and 6) possible easier material penetration due to the presence of energy at different frequencies. There are numerous applications of the UWB system, such as personal area networks (PANs), sensor networks, geo-location sensors, and emergency communications. An overview of the ranges for typical applications is given Table 1.1.

Table 1.1: Typical environment and ranges for UWB applications

Environment	Range
Indoor residential	1-30m
Indoor office	1-100m
Body area network	0.1-2m
Outdoor peer to peer	1-100m
Outdoor base station scenario	1-300m
Industrial environments	1-300m
Emergency communications	1-50m

1.2 UWB channel standard model

1.2.1 IEEE 802.15.3a

The IEEE established the 802.15.3a study group to define a new physical layer concept for short range, high-data-rate applications. The purpose of the study group is to provide a higher speed PHY for the existing approved 802.15.3a standard for applications which involve imaging and multimedia. The main desired characteristics of the alternative PHY are:

- Coexistence with all existing IEEE 802 physical layer standards;
- Target data rate in excess of 100 Mbps for consumer applications;
- Robust multipath performance;
- Location awareness;
- Use of additional unlicensed spectrum for high data rate WPANs (wireless personal area network)

1.2.1 IEEE 802.15.4a

The IEEE established the 802.15.4a study group to define a new physical layer concept for low data rated applications utilizing UWB technology at the air interface. The study group addresses new applications that require only data throughput, but long battery life such as low-rate wireless personal area network, sensors and small networks.

1.3 Motivation

In this thesis, indoor office is considered, especially line-of-sight (LOS) environments such as classrooms and office. UWB systems that use relatively large bandwidth must use low power so as not to cause interference to the neighboring communication systems. This feature allows the UWB system to be deployed in line-of-sight (LOS) and slightly cluttered non-line-of-sight (NLOS) environments in which the signal undergoes small attenuation. In these environments, the UWB channel largely depends on surroundings of the transmitting (Tx) and receiving (Rx) antennas. The presence of human bodies might be a dominant factor that can alter such channel. In this dissertation, we analyze the effect of human body on UWB channel in indoor LOS environments and propose the channel model including human body effects.

Chapter 2 deals with UWB channel variation depending on the number of people in indoor LOS environments. Many researches about the effects of human bodies on wireless propagation channels have been reported until recently [2]-[11], however they dealt with channel variation by a single person. Some studies on the channel variation in populated environments were reported [12]–[14], but they did not consider the channel variation with population density. And the study [14] dealt with the channel variation depending on how many seats are occupied by passengers in airplane, not indoor environment. In this chapter, we analyzed UWB channel variation with population density in indoor LOS environment and proposed the channel model with population density. To assess variation of UWB channels, we choose four environments, and consider the following four scenarios in each environment: 1) no people, 2) 25% of maximum number of people, 3) 50%, and 4) 100%. Because the UWB system has an extremely wide bandwidth compared to conventional wireless system, it is necessary to understand the frequency correlation characteristics of UWB channels. To show the frequency correlation characteristics of UWB channels, a frequency correlation coefficient of the measured channel gains is first analyzed. And a distance-dependent path-loss model, a frequency-dependent path-loss model, and time dispersion parameters are considered. To obtain a frequency-dependent path-loss model, the result of the frequency correlation coefficients and the same method of [15] are used. To provide a general channel model, the linear regression model with population

density for each parameter is obtained.

In chapter 3, small-scale amplitudes statistics in the absence and presence of human bodies are measured in indoor LOS environments and a statistical model of the small-scale fading distribution is proposed. Many previous studies dealt with the shadowing effect of human bodies on the UWB channel [13], [16]-[19], but no study has dealt with small-scale fading in the presence of human bodies. In [20]–[23], which did not consider human bodies, the small-scale fading distribution was matched to some typical theoretical distributions such as Lognormal, Nakagami, Rayleigh, Rice, and Weibull distributions depending on the measurement environments and scenarios. In this chapter, we measure and analyze the small-scale fading distribution in the absence and the presence of human bodies. To obtain the small-scale amplitudes statistics, we consider a situation where either LOS path is not blocked or slightly blocked by human bodies as a Rx is shifted by small-scale (1λ) distance while a Tx is fixed. To create this situation, we set the height of the Tx and Rx antennas in consideration of the height of human bodies sitting on chairs. In this situation, the effects of human bodies on all paths including LOS path are different depending on where the Rx is located. From the measured UWB channel data, an impulse response is obtained by inverse Fourier transform which is used to transform the measured frequency domain data to the time domain data. The extraction of amplitude for each bin was carried out by collecting a vector of 49 amplitude values with an equivalent delay at 49 local points. To evaluate the goodness-of-fit for these candidate amplitude distributions, we use the Kolmogorov-Smirnov and chi-square hypothesis tests. These two tests compare empirical data and a reference probability distribution. Due to some limitations in each of these two hypothesis tests, both tests are deployed in this chapter to ensure the reliability of the fitting. From the results of two tests, we found the distribution well fitted to the small-scale fading amplitude statistics and proposed the model for the parameters of the distribution. The proposed model is used to analyze the effect of human body on the performance of UWB system in the next chapter.

In chapter 4, impulse radio (IR) UWB system is briefly introduced. IR-UWB system does not require frequency up-conversion and down-conversion because the system communicates with baseband pulses of very short duration. Due to their fine time resolution, the receiver structure

consists of a number of correlators that are sampled at the delays related to specific number of multipath components; each of those correlators is known as rake finger. In this chapter, we analyzed bit-error-rate (BER) performance of the Rake receiver in IR-UWB system, using the proposed channel models in Chapter 3, comparing with previous standard channel model, i.e., IEEE 802.15.4a [24], and also considering People Shadowing Effect (PSE) [19]. Among several channel models of 802.15.4a, CM 3 channel model which consider scenarios in indoor office environment is used in the performance analysis. PSE model describes the scenario when a person moves along a straight line perpendicular to the LOS path. The PSE model provides a suitable way to determine the shadowing term instead of using an independent log-normal distributed random variable which is used in 802.15.4a CM 3 model. In this chapter, 6 different channel models are utilized in BER performance analysis.

1.4 Dissertation Outline

This dissertation is organized as follows: Chapter 2 deals with the modeling of UWB channel with population density in indoor LOS environments. In Chapter 3, the small-scale fading distribution in the absence and the presence is proposed. And Chapter 4 analyzed BER performance of Rake receiver based on Chapter 3. Finally, Chapter 5 summarizes and suggests future research directions.

Chapter 2. Modeling of UWB channel with Population density in indoor LOS environments

2.1 Introduction

In indoor environments (including a classroom), a human body is a major factor that changes channel characteristics. So, many researches about the effects of human bodies on wireless propagation channels have been reported until recently. They can be divided into three types: 1) the depth and duration of shadow fading due to pedestrians moving near to the transmitter and the receiver [2]–[4], 2) the effect of human bodies on wireless personal area networks (WPANs) in which one end of the link is located either close to or on a person [5]–[8], and 3) the effect of a human body on wireless body area networks (WBANs) in which both ends of the link are located either close to or on a person [9]–[11].

The above-mentioned articles dealt with channel variation by a single person. Several studies on the channel variation in populated environments were reported [12]–[14]. In [12], authors dealt with the time-varying property of the channel response due to moving human bodies. The paper provides the full response on a given link of which each path as the sum of a static one predicted using site-specific ray tracing plus zero-mean time-varying one, based on some type of empirical model. The probability model for the shadowing due to human activities was proposed in [13]. These two papers considered the channel variation in the populated environments, but they did not consider the channel variation with population density. Another study [14] assessed the channel variation depending on how many seats are occupied by passengers in airplane, but this environment mostly composed by metal materials is uncommon and very different from building environments.

This chapter addresses UWB channel variation depending on the number of people in indoor LOS environments. To assess variation of UWB channels, we choose four environments, and consider the following four scenarios in each environment: 1) no people, 2) 25% of maximum number of people, 3) 50%, and 4) 100%. First, a frequency correlation coefficient of the

measured channel gains is analyzed. We deal with a distance-dependent path-loss model, a frequency-dependent path-loss model, and time dispersion parameters. To provide a general channel model, we obtained the linear regression model with population density for each parameter.

This chapter is organized as follows: Section 2.2 presents the channel measurement system and the measurement scenario. In Section 2.3, a frequency correlation coefficient of the measured channel gains is analyzed. Section 2.4 shows path-loss characteristics. In Section 2.5, the time dispersion parameters are described. Finally, the paper is ended with a summary and conclusion in Section 2.6.

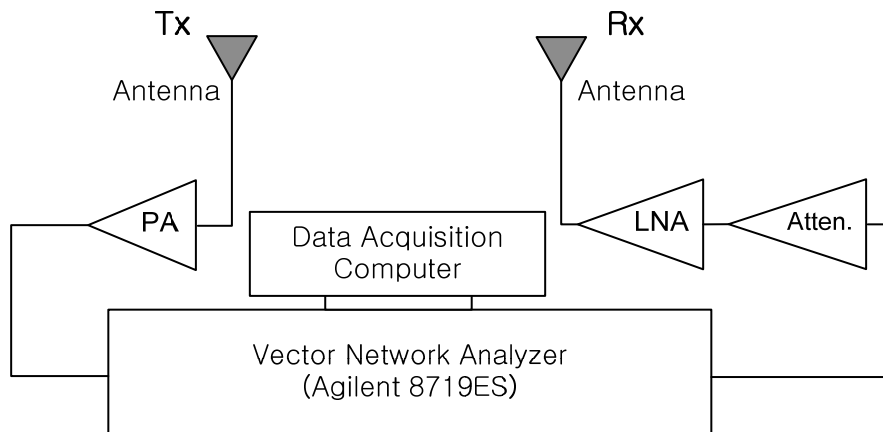


Figure 2.1: Block diagram of the measurement system

2.2 Measurement methodology

2.2.1 Measurement system

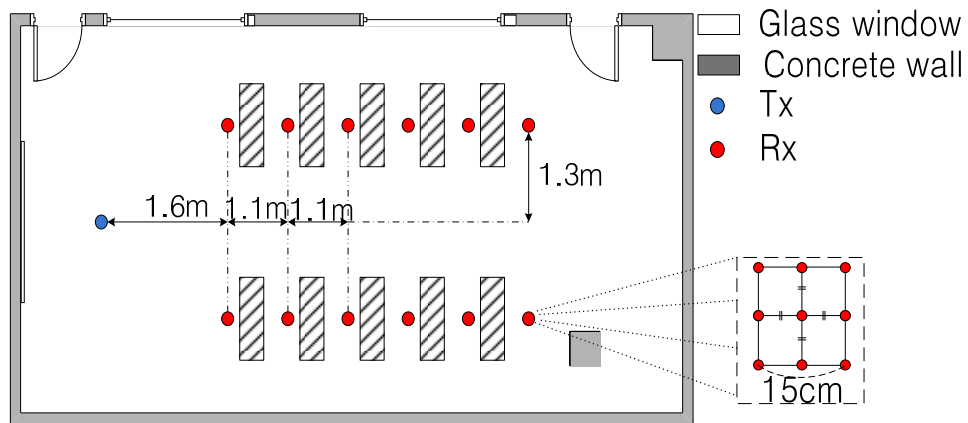
We measured the UWB channel using the frequency-domain channel sounding method with a vector network analyzer (VNA). The VNA (Agilent 8719ES) transmits 1601 discrete tones that are uniformly spaced from 3.0 to 4.6 GHz, requiring 400 ms for one sweep. This frequency interval allows us to measure a multipath with a maximum excess delay of 500 ns, and the bandwidth of 1.6 GHz gives a time resolution of 0.625 ns. The measurement system is described in Figure 2.1. The same dipole antennas with a gain of 2 dBi are used on both the transmitter and receiver sides and are located on 1.2-m-high tripods. The power amplifier (PA) with the gain of 25dB and the low-noise amplifier (LNA) with the gain of 27 dB are used. To eliminate the effect of antennas, PA, LNA, and cables, the measurement system is calibrated in an anechoic chamber.

2.2.2 Measurement Scenario

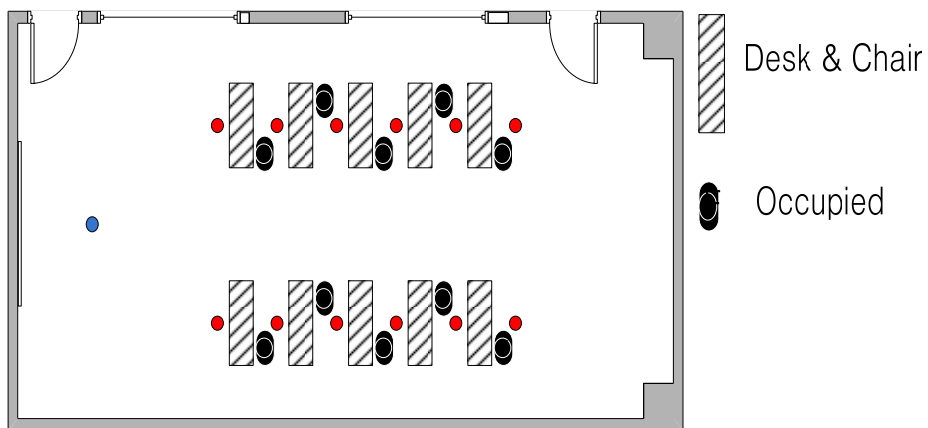
To analyze the effect of people on UWB channels in indoor LOS environments, we measured channels in four environments which have different room sizes and wall structures. Size, area, maximum number of people, and main features are described in Table 2.1. The ceiling heights of all environments are 2.7m. In each environment, four scenarios are considered: no people, 25% of the maximum number of people, 50%, and 100%. During measurements, people did not move around, but were just sitting on their chair with small motion if necessary. In each scenario, we measured the channel at several receiving points from the fixed transmitting point in the environment. At each receiving point, the receiver was moved around to 9 local positions to obtain a local average. Figure 2.2 shows the floor plans for no people and 10 people in B environment. In Figure 2.2 (b), 10 people are sitting on their chairs in zigzags. In the other environments, people take their seats in the same way as in Figure 2.2 (b).

Table 2.1: Size, Area, Max. No. of people, and Main features

Environment	Size [m] (L x W)	Area [m^2]	Max. No. of people	Main features
A	7.6 x 4.6	34.96	16	- Glass window (on the opposite side of Tx) - Blackboard (on the same side of Tx)
B	10.8 x 5.2	56.16	20	- Two metal doors (front and rear side) - Two big glass windows (on the left side of Tx)
C	12.4 x 6.8	84.32	24	- Glass window (on the same side of Tx) - Metal doors (on the opposite side of Tx) - Blackboard (on the left side of Tx)
D	9.5 x 7.3	69.35	24	- Metal wall and glass window (on the left side of Tx) - Metal door (on the opposite side of Tx)



(a)



(b)

Figure 2.2: Floor plans for (a) no people and (b) 10 people in B environment.

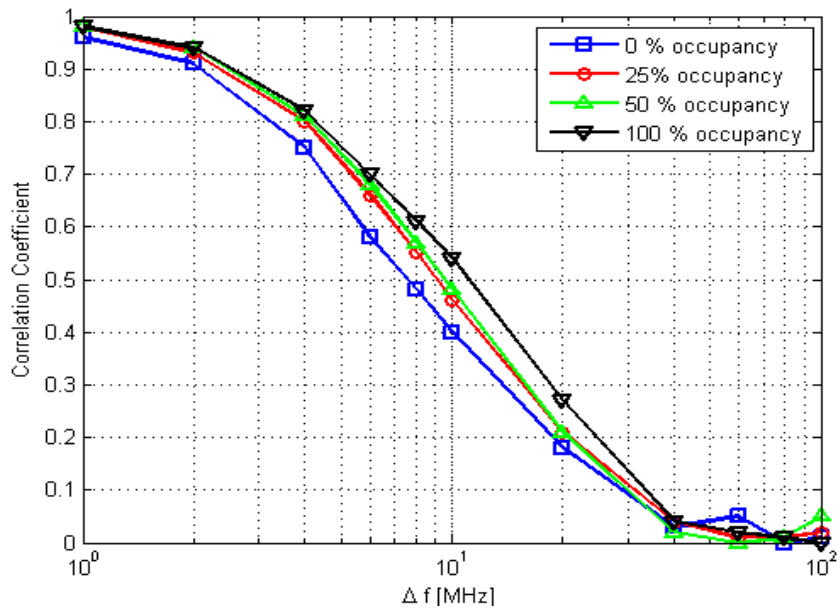
2.3 Frequency Correlation Coefficient of the Measured Channel Gains

Because the UWB system operates in an extremely wide bandwidth compared to conventional wireless systems, it is necessary to understand the frequency correlation characteristics of UWB channels. To characterize the frequency correlation properties, the correlation coefficient is used to represent the correlation level of the received signal amplitudes between frequency tones. It is represented as [25]

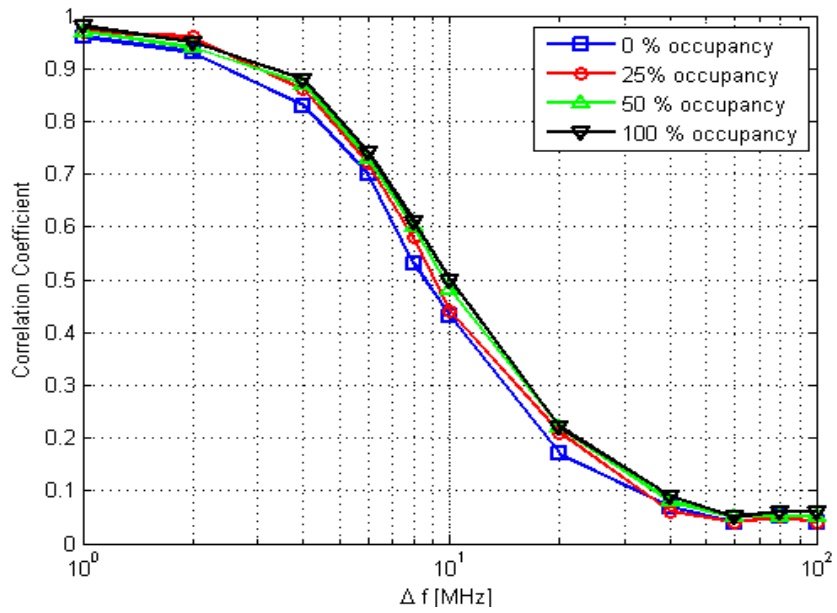
$$\rho(\Delta f) = \frac{C(f, f + \Delta f)}{\sqrt{C(f, f)}\sqrt{C(f + \Delta f, f + \Delta f)}} \quad (2.1)$$

where $C(f_1, f_2) = E[\{a(f_1) - m(f_1)\}\{a(f_2) - m(f_2)\}]$, $a(f_1)$ is the amplitude of the channel gain at frequency f_1 , and $m(f_1)$ is the mean of $a(f_1)$.

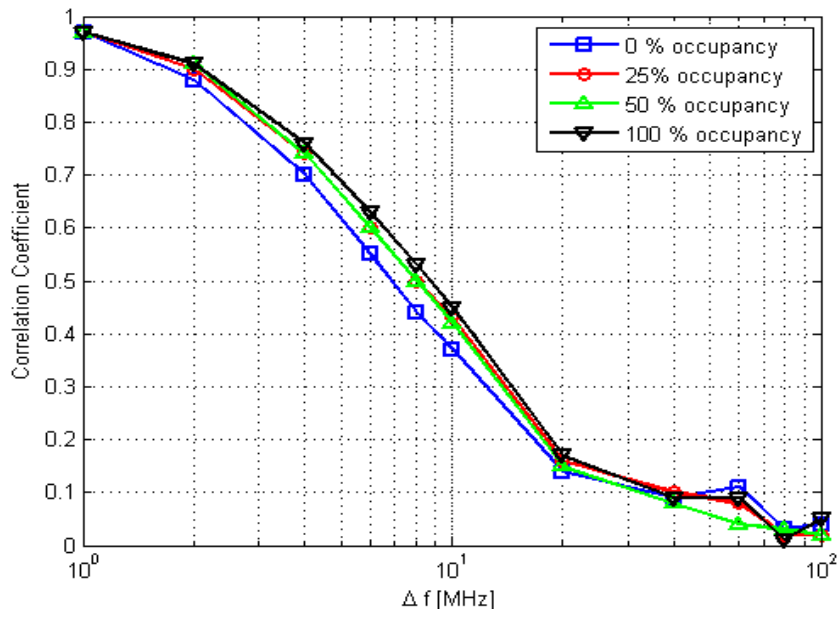
Figure 2.3 shows the correlation coefficient of the measured channel gains in all environments. There are differences of the correlation among all environments, which is because of different size and different main features shown in Table 2.1, but the correlation increases as more people exist in all environments. As the numbers of people in the environment increases, more multipath are blocked or weakened by existing people. This results in increasing correlation of the measured channel gains. In all environments, the correlation coefficients between two frequency tones with an interval of $\Delta f = 10\text{MHz}$ are mostly smaller than 0.5. This result is used in calculating the frequency-dependent path-loss model in section 2.4.2.



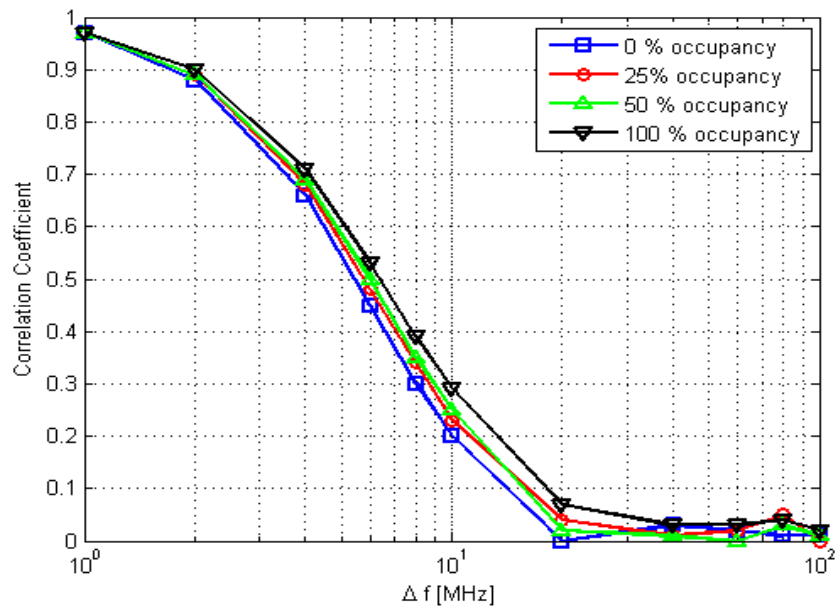
(a)



(b)



(c)



(d)

Figure 2.3: Correlation Coefficient with Δf in (a) Environment A, (b) Environment B, (c) Environment C, and (d) Environment D

2.4 Path-Loss Characteristics

2.4.1 Empirical distance-dependent path-loss model

This section shows the path-loss model with distance. We assume that the distance dependence of the path-loss follows the log-distance model with lognormal shadowing as conventional narrowband models. The distance dependent path-loss model is given by,

$$PL_{dB}(d) = PL_{dB}(d_0) + 10n \log_{10}(d / d_0) + \varepsilon_d \quad (2.2)$$

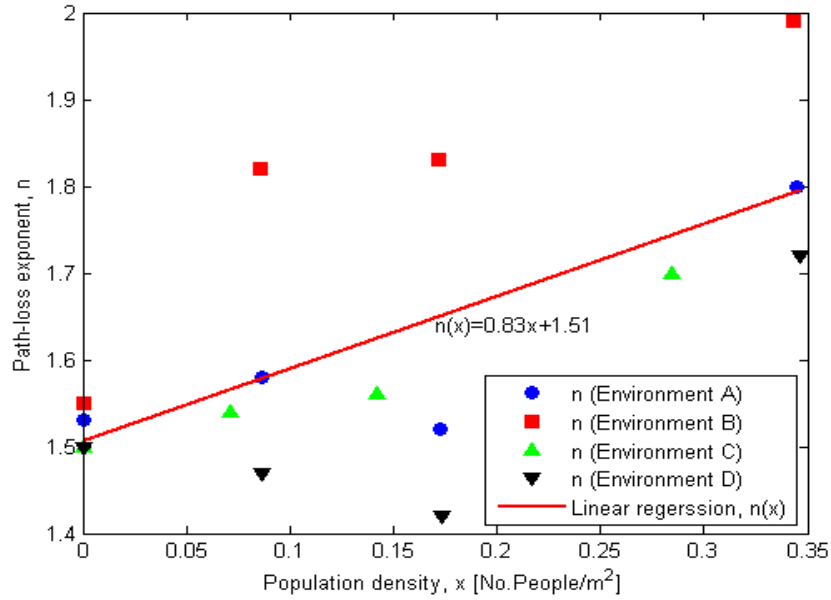
where $PL_{dB}(d_0)$ is the path-loss at the reference distance $d_0 = 1m$, d is the separation between the transmitter and the receiver, n is the distance-dependent path-loss exponent, and ε_d is a random variable in dB related to the degree of large-scale fading to follow the zero-mean Gaussian distribution with standard deviation of σ_d [26]. $PL_{dB}(d_0)$ and σ_d in (2.2) are averaged over 1.6GHz bandwidth, and n is computed using the minimum mean square error fitting. These parameters are summarized in Table 2.2. The path-loss exponent n for the scenario with no people in the environment is 1.5 to 1.55 which is similar to the results of the previous studies [27]-[30]. The path-loss exponent becomes larger as more people exist. In particular, for B environment, the exponent becomes 1.99 when all seats are occupied by human bodies. As described in Table 2.1, B environment has two big glass windows, which cause more path-loss compared to the other environments. But D environment has the smallest exponent because there is a wall of metal surface. Because of different room size and wall structures, there are some differences of the exponent among environments.

In all environments, the exponent n increases from 0.2 up to 0.44 with varying number of people. To provide a general distance-dependent path-loss model, we obtained the linear regression model with population density defined as the number of people per unit area ($[m^2]$). Figure 2.4 (a) shows the path-loss exponents and its regression model. For all environments, the linear regression model is $n(x) = 0.83x + 1.51$, where x is the population density. The

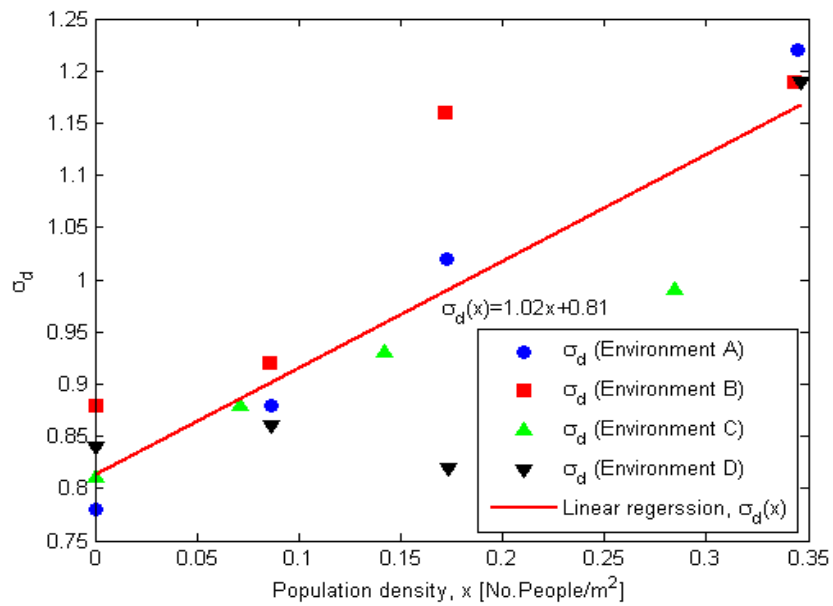
Table 2.2: Empirical Distance-dependent Path-loss Parameters

	A			B			C			D		
	n	$PL_{dB}(d_0)$ [dB]	σ_d [dB]	n	$PL_{dB}(d_0)$ [dB]	σ_d [dB]	n	$PL_{dB}(d_0)$ [dB]	σ_d [dB]	n	$PL_{dB}(d_0)$ [dB]	σ_d [dB]
0%	1.53	44.50	0.78	1.55	45.47	0.80	1.50	43.34	0.81	1.50	44.39	0.84
25%	1.58	44.72	0.88	1.82	44.14	0.92	1.54	43.28	0.88	1.47	44.68	0.86
50%	1.52	45.43	1.02	1.83	45.71	1.16	1.56	43.50	0.93	1.42	44.91	0.82
100%	1.80	44.17	1.22	1.99	45.12	1.19	1.70	42.94	0.99	1.72	43.33	1.19

standard deviation σ_d and its linear regression model with population density are shown in Figure 2.4 (b). In the figure, σ_d is heavily dependent on the population density and the regression model of σ_d is $\sigma_d(x) = 1.02x + 0.81$. As the population density increases, both the path-loss exponent and the standard deviation get larger.



(a)



(b)

Figure 2.4: (a) Path-loss exponent n and (b) σ_d .

2.4.2 Empirical frequency-dependent path-loss model

For the frequency-dependent path-loss model, we used the following equation,

$$PL_{dB}(f) = PL_{dB}(f_c) + 20k \log_{10}(f / f_c) + \varepsilon_f \quad (2.3)$$

where $f_c = 3.8$ GHz is the reference frequency, k is the frequency-dependent path-loss exponent expressing the dependence on frequency, and ε_f is a zero-mean Gaussian distributed random variable (in dB) with a standard deviation of σ_f also in dB.

For the calculation of the frequency-dependent path-loss exponent k , the same method of [15] is used in this paper. We used the minimum mean square error fitting, using the distance-averaged path-loss values for each frequency. The critical point here is to model the large-scale characteristics of the environment. The method needs to determine how the pathloss increases with frequency, although it does not show rapid variations in the path-loss for consecutive frequency samples, i.e., the frequency selectivity of the channel. Therefore, the method needs to obtain the local mean values computed by independent frequency samples. These local mean values were used for the calculation of the k in (2). From [31], the number N of independent samples required to estimate the local mean with 90% degree of confidence for ± 1 dB deviation around the true mean is 57. Therefore, we need to estimate the rate of decorrelation of the samples, i.e., the number of consecutive frequency samples that are needed so that the autocorrelation of the channel transfer function (CTF) falls below the threshold value of 0.5. In this letter, 10 samples (MHz) are chosen to meet this condition in our most scenarios. Having estimated this value, the averaging window size of samples used to calculate the local means is given by multiplying this value with the number of independent samples $N = 57$, i.e., $10 \times 57 = 570$ samples. This window is slid by 10 MHz for the computation of the next local mean, and the procedure continues to the end of the frequency samples. Figure 2.5 depicts the above method to obtain the frequency dependent path-loss model.

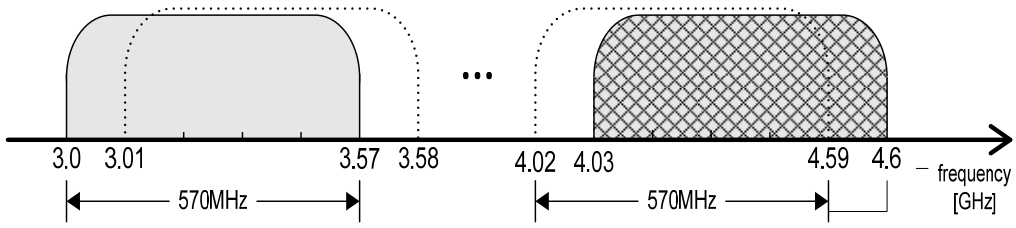
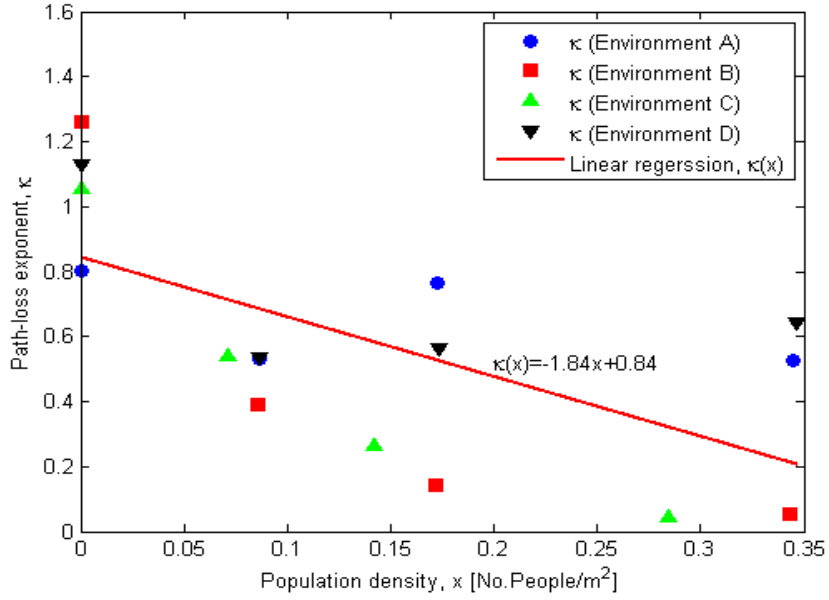


Figure 2.5: Methods for obtaining frequency-dependent path-loss model

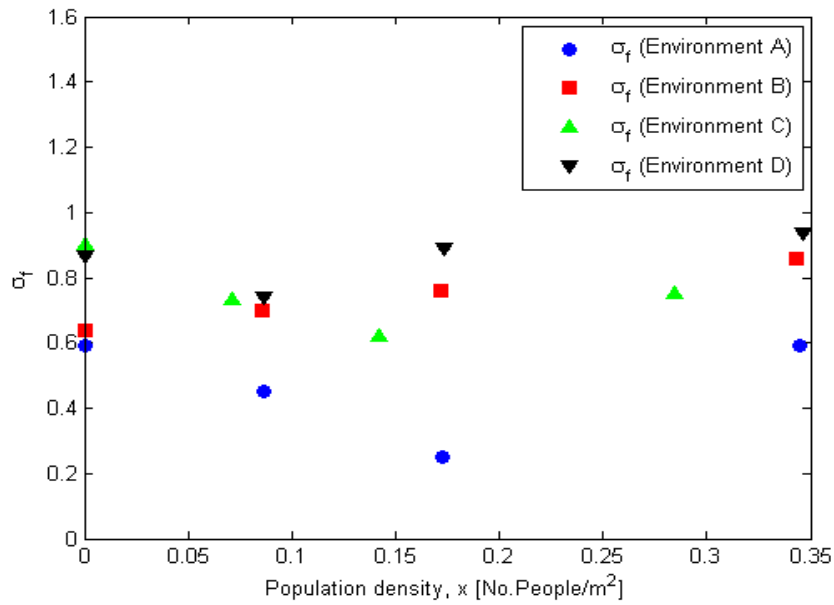
Using the above method, we obtained the parameters of (2.3) which are listed in Table 2.3. The path-loss exponent k decreases as the number of people increases. This means that the attenuation of the frequency-dependent path-loss $PL_{dB}(f)$ with frequency tones becomes smaller as more people exist in the environment. Like the distance-dependent path-loss exponent, the exponent k depends on the environments. For a general model of the frequency-dependent path-loss model, we obtained the linear regression model with a function of population density. Figure 2.6 (a) shows the path-loss exponent k and its linear regression model with population density. The regression model of k is $\kappa(x) = -1.84x + 0.84$. As population density increases, the path-loss exponent k becomes smaller. Unlike the result of σ_d in Figure 2.6 (b), the standard deviation σ_f is irrelevant to population density, which is shown in Figure 2.4 (b).

Table 2.3: Empirical Frequency-dependent Path-loss Parameters

	A			B			C			D		
	k	$PL_{dB}(f_c)$ [dB]	σ_f [dB]	k	$PL_{dB}(f_c)$ [dB]	σ_f [dB]	k	$PL_{dB}(f_c)$ [dB]	σ_f [dB]	k	$PL_{dB}(f_c)$ [dB]	σ_f [dB]
0%	0.80	52.65	0.59	1.26	53.37	0.64	1.06	52.74	0.90	1.13	52.90	0.87
25%	0.53	52.39	0.45	0.39	53.35	0.70	0.54	51.64	0.73	0.54	52.87	0.74
50%	0.76	52.31	0.25	0.14	52.40	0.76	0.26	51.72	0.62	0.57	52.93	0.89
100%	0.52	51.24	0.59	0.06	52.41	0.86	0.04	51.89	0.75	0.64	52.45	0.94



(a)



(b)

Figure 2.6: (a) Path-loss exponent k and (b) σ_f .

2.5 Time-Dispersion Parameters

In this section, two time-dispersion parameters are considered, i.e., the mean excess delay and the rms delay spread. The signal measured using a VNA is a frequency response. The inverse Fourier transform (IFFT) is used to transform the measured frequency domain data to the time domain. First, the pass-band signal is obtained with zero padding from the lowest frequency down to DC, taking the conjugate of the signal, and reflecting it to the negative frequencies. The result is then transformed to the time domain using IFFT.

The mean excess delay is the first moment of the power delay profile and is defined as follows:

$$\bar{\tau} = \frac{\sum_k P(\tau_k) \tau_k}{\sum_k P(\tau_k)} \quad (2.4)$$

The RMS delay spread is the square root of the second central moment of the power delay profile and is defined as

$$\sigma_\tau = \sqrt{\overline{\tau^2} - (\bar{\tau})^2} \quad (2.5)$$

where

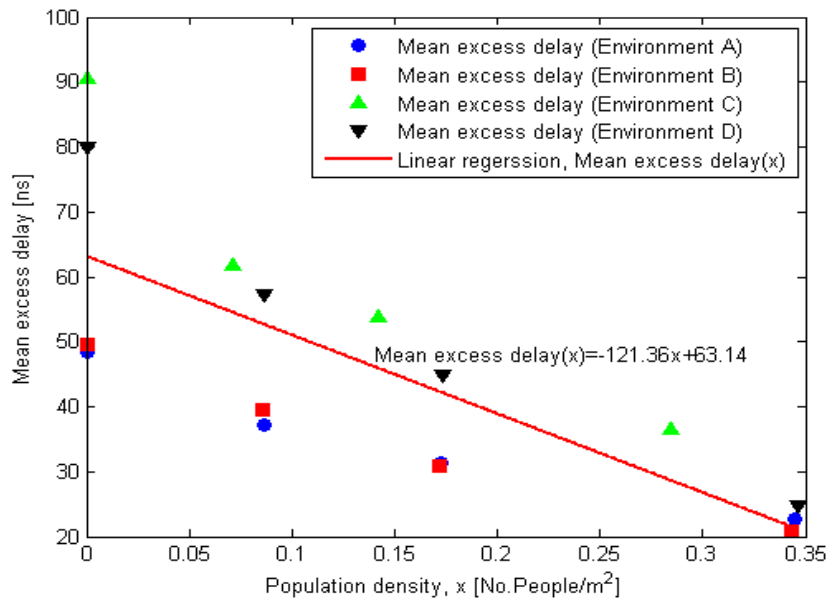
$$\overline{\tau^2} = \frac{\sum_k P(\tau_k) \tau_k^2}{\sum_k P(\tau_k)} \quad (2.6)$$

These delays are measured relative to the first detectable signal arriving at the receiver at τ_0 .

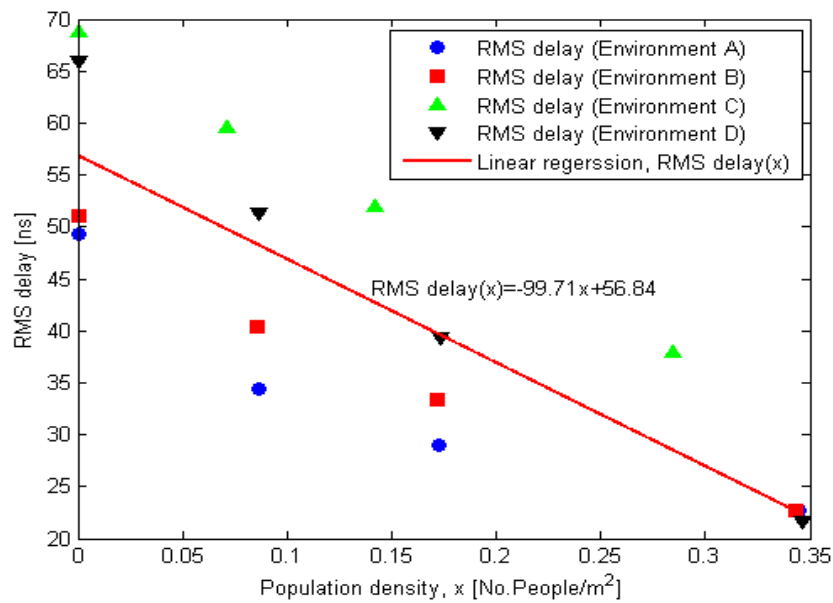
Equations (2.4)-(2.6) do not rely on the absolute power level of $P(\tau)$, but only on the relative amplitudes of the multipath components (MPCs) [26].

Figure 2.7 shows the mean excess delay and RMS delay spread with population density. For a

general model of time dispersion parameters, we obtained the linear regression models shown in the figure. As population density increases, the delay spread parameters decrease, which is explained by the fact that more multipath are blocked or weakened due to the people. This phenomenon is depicted in Figure 2.8. Figure 2.8 (a) and (b) show the normalized power delay profiles (PDP) in B and D environment, respectively. The difference of the normalized PDPs between 0 and 100% occupancy in B environment is smaller than in D environment, and this leads to decreased delay parameters. Like the results of [14] in the airplane, the delay spread parameters get smaller as more people exist. But the parameters are larger than those in the airplane [14], because the indoor environments have different materials and structures compared to the airplane which mainly consists of metallic surfaces. As there are more people in the environment, some multipath with large delay time are weakened by human bodies. As a result, the amplitudes of the multipath components get smaller. From Figure 2.7-8, as more people exist in the environment, more multipath are blocked, which results in less dispersive channel.

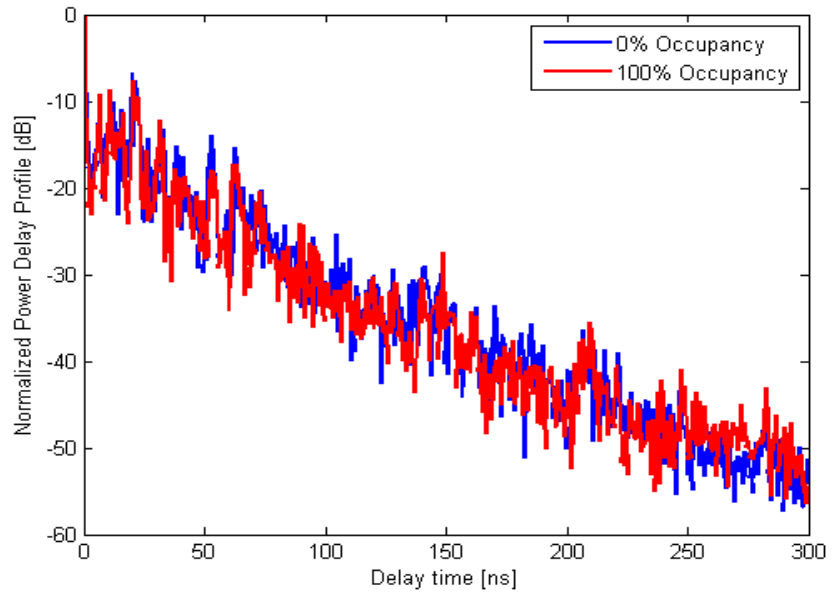


(a)

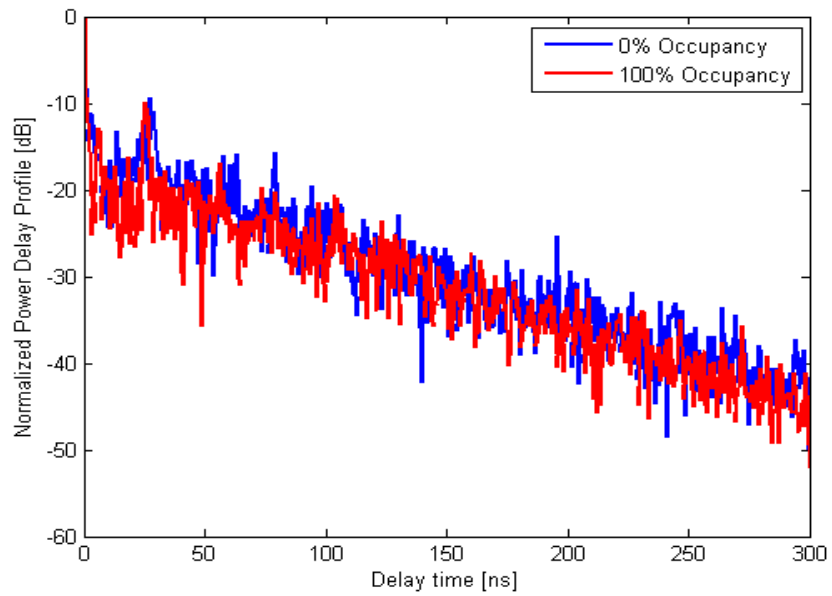


(b)

Figure 2.7: (a) Mean excess delay and (b) RMS delay spread



(a)



(b)

Figure 2.8: Normalized power delay profile in (a) B and (b) D environment

2.6 Conclusions

To show the effect of the presence of people in indoor LOS environments on a UWB channel, the measurements are carried out in four environments which have different size and structure. For each environment, four scenarios which have different number of people are chosen. The frequency-domain channel sounding method was used for channel characterization from 3.0 to 4.6 GHz. In this chapter, four UWB channel parameters are considered, i.e., the frequency correlation coefficient of the measured channel gains, the distance-dependent path-loss model, frequency dependent path-loss model, and time dispersion parameters. As increasing the number of people, the frequency correlation coefficients get larger. For the distance-dependent path-loss model, frequency dependent path-loss model, and time dispersion parameters, the linear regression model with a function of population density to obtain a general model for each parameter. The distance-dependent path-loss exponent becomes larger due to larger path-loss with increasing population density, while the frequency-dependent path-loss exponent becomes smaller. For the time dispersion parameters, the mean excess delay and RMS delay spread get smaller as population density increases. This means that the UWB channel becomes less dispersive with increasing population density. This is because more multipath are blocked or weakened by increasing the number of people. In summary, this paper shows that the presence of people substantially affects radio-wave propagation in indoor LOS environments and should be considered when characterizing the performance of UWB systems. This finding will be helpful to those who want to validate the results of software simulations of radio-wave propagation in indoor LOS environments.

Chapter 3. Human Body Affected Small-Scale Fading for Indoor UWB channel

3.1 Introduction

The presence of human bodies might be a dominant factor that can alter such channel. Many previous studies have dealt with the shadowing effect of human bodies on the UWB channel [13], [16]–[19], but no study has dealt with small-scale fading in the presence of human bodies. In [20]–[23], which did not consider human bodies, the small-scale fading distribution was matched to some typical theoretical distributions such as Lognormal, Nakagami, Rayleigh, Rice, and Weibull distributions depending on the measurement environments and scenarios. In this paper, we measure and analyze the small-scale fading distribution in the absence and the presence of human bodies.

The IEEE 802.15.4a UWB channel model [24] is commonly used in performance analysis, but the model does not include the small-scale fading variation in the presence of human bodies as well as the shadowing effect of human bodies on the UWB channel. Therefore, it is expected that there are distinct differences in UWB system performance if the human body effect on the channels is included.

In this paper, we considered a situation where either LOS path is not blocked or slightly blocked by human bodies as a Rx is shifted by small-scale (1λ) distance while a Tx is fixed. To create this situation, we set the height of the Tx and Rx antennas in consideration of the height of human bodies sitting on chairs. In this situation, the effects of human bodies on all paths including LOS path are different depending on where the Rx is located.

The main contribution of this chapter is that we measure the small-scale amplitude statistics in the absence and presence of human bodies and propose a statistical model of the small-scale fading distribution.

The remainder of the chapter is organized as follows: Section 3.2 presents the channel measurement system and measurement scenario. In Section 3.3, we describe the small-scale

fading distribution in the absence and the presence of human bodies. Finally, Section 3.4 presents the summary and the conclusion.

3.2 Measurement Campaign

3.2.1 Measurement system

In this chapter, we measured the UWB channel using a frequency-domain channel sounding method for channel characterization with the vector network analyzer (VNA). The VNA (Agilent 8719ES) transmits 1601 discrete tones that are uniformly spaced from 3.0 to 4.6 GHz with a frequency interval of 1 MHz, requiring 800 ms for one sweep. This frequency interval allows us to measure a multipath with a maximum excess delay of 1000 ns, and the bandwidth of the system yields a time resolution of 0.2174 ns. The measured data from the VNA were stored on a data acquisition computer via a general purpose interface bus (GPIB). The measurement system is the same described in Section 2.2.1. The same dipole antennas with a gain of 2 dBi are used on both the transmitting and receiving sides. We set the height of both a Tx and Rx antennas as 1.2m in consideration of the height of a human body sitting on a chair, which is mostly from 0.9 to 1.2m. The height of the antennas is chosen to consider a situation where either LOS path is not blocked or slightly blocked by human bodies as the Rx is shifted by small-scale (1λ) distance while the Tx is fixed. A power amplifier (PA) with a gain of 25dB and a low-noise amplifier (LNA) with a gain of 27 dB are used on the transmitting and receiving sides, respectively. To eliminate the effect of the antennas, the PA, the LNA, and the cables, all measured data were calibrated in the anechoic chamber.

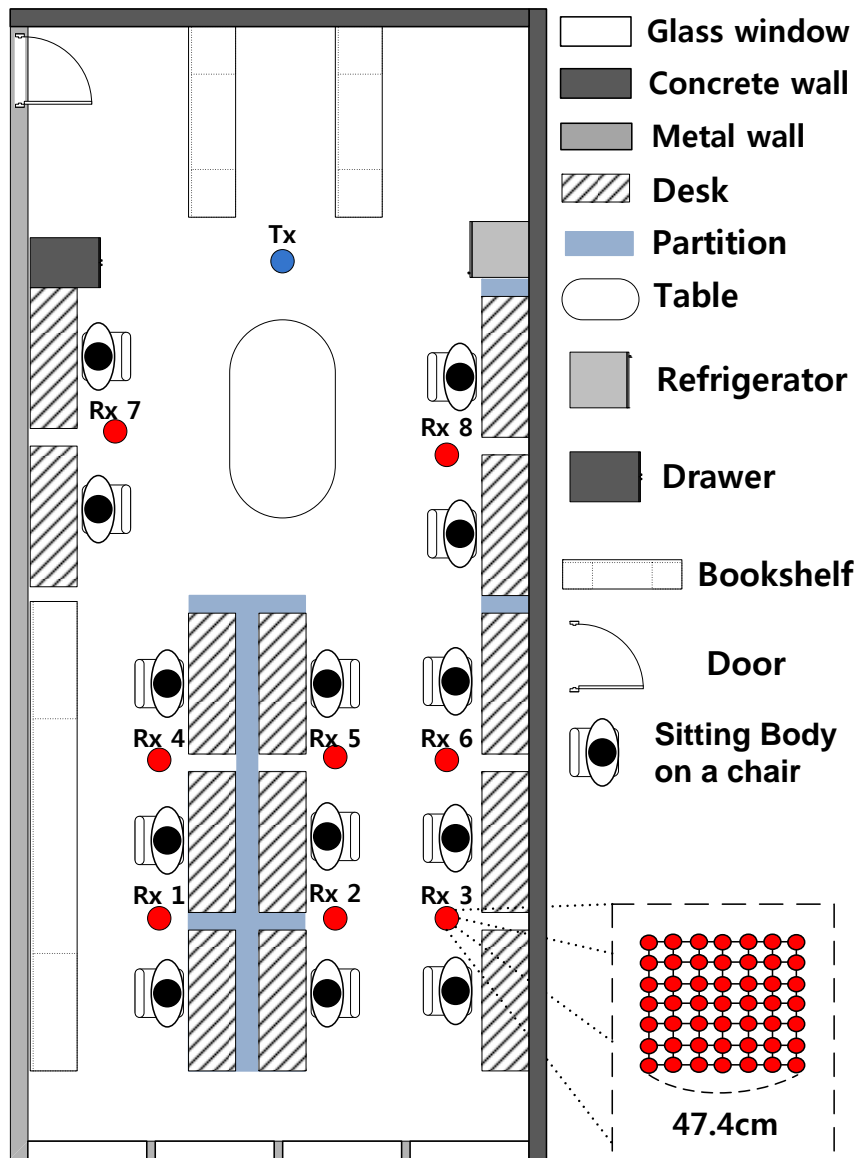
3.2.2 Measurement scenario

In this chapter, we consider five representative environments for the analysis of small-scale fading in the absence and presence of human bodies in indoor LOS environments. The details of five environments are shown in Table 3.1. The floor plans which include the transmitter,

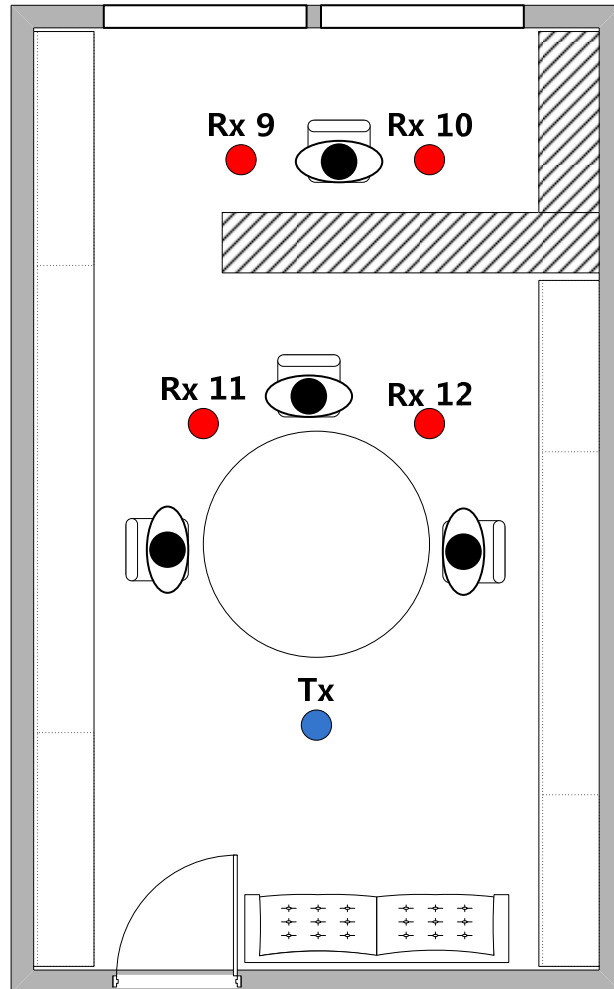
receiver, and positions of the human bodies are described in Figure 3.1. In order to determine the small-scale fading statistics, a sufficient number of measurement points have to be taken in an area where large scale parameters such as shadowing are constant [1]. With these requirements, we choose 49 (7×7 grid) local measurement points with 1λ of distance between two neighboring local points, corresponding to 3.8 GHz, which is the center frequency of the measurement frequency bands. During the measurement in all environments, human bodies did not move around, but were just sitting on their chair with small motion.

Table 3.1: Size and Main Features of all Environments

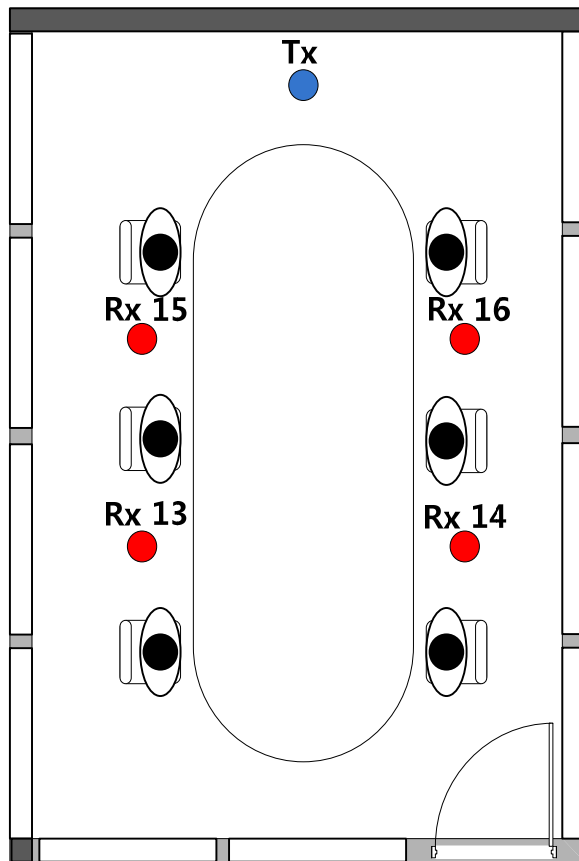
	Size [m] (L x W)	Main features
Environment 1	14.4 x 5.8	- Partition (height: 1m) - Glass window - Bookshelves
Environment 2	6.2 x 3.4	- Metal wall (two side) - Glass window - Bookshelves - Round table
Environment 3	5 x 2.8	- Glass walls (2 sides) and widow - Conference table - Glass door
Environment 4	12.6 x 10.4	- Partition (height: 1.8m) - Glass windows (2 sides)
Environment 5	8 x 3.5	- Metal wall (one side) - Partition (height: 1m) - Glass windows (2 sides) - Bookshelves



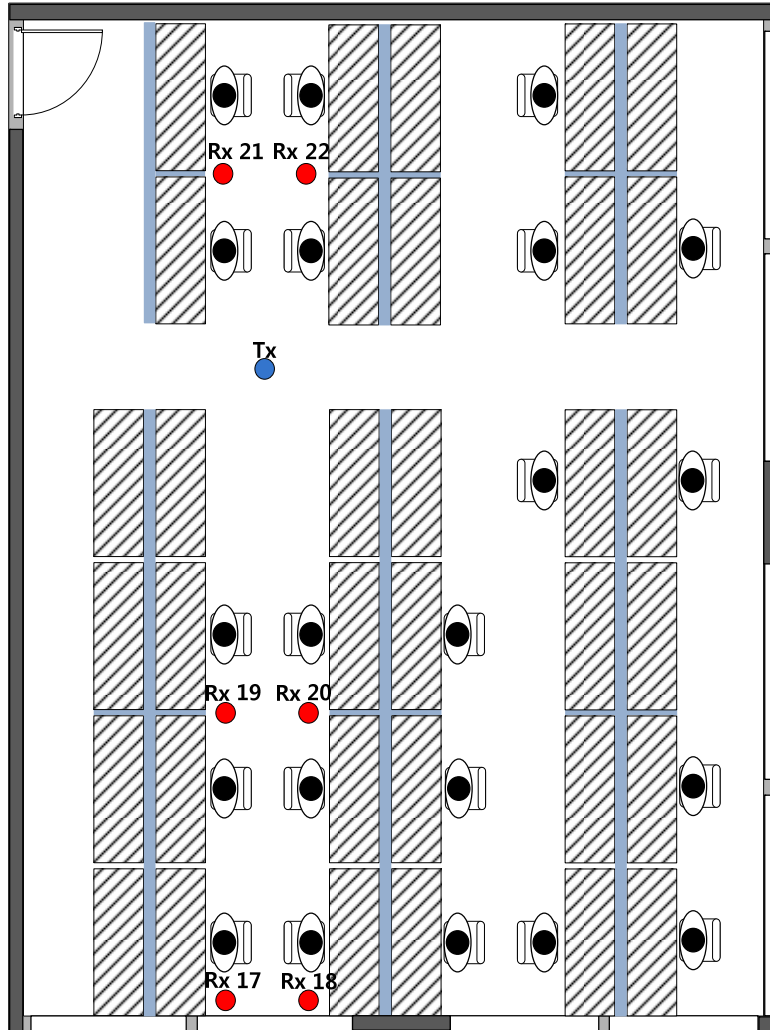
(a)



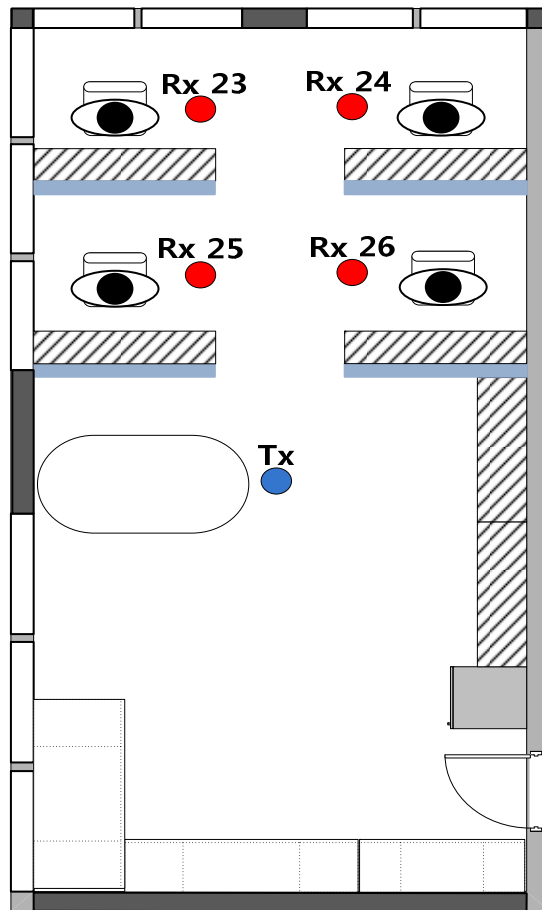
(b)



(c)



(d)



(e)

Figure 3.1: Floor plans for (a) Environment 1, (b) Environment 2, (c) Environment 3, (d) Environment 4, and (e) Environment 5

3.3 Statistical Modeling of Small-Scale Fading [1]

In narrowband systems, many MPCs fall into each resolvable delay bin, so that the central limit theorem is applicable, and the amplitudes of the bins exhibit a Rayleigh distribution. In UWB system, the number of MPCs falling into each resolvable bin is much smaller because of fine timing resolution, and it has been empirically determined that in many environments, alternative amplitude distributions must be used:

1) Nakagami distribution: Observed in

$$f(x) = \frac{2}{\Gamma(m)} \left(\frac{m}{\Omega}\right)^m x^{2m-1} \exp\left(-\frac{m}{\Omega} x^2\right) \quad (3.1)$$

where $m \geq 1/2$ is the Nakagami m -factor, $\Gamma(m)$ is the gamma function, and Ω is the mean-square value of the amplitude. The m -parameter is often modeled as a random variable.

2) Rice distribution: The Rice distribution describes the envelope of a sum of one dominant component and many smaller components.

3) Lognormal distribution: This distribution has the advantage that the fading statistics of the small-scale statistics and the large-scale variations have the same form; the superposition of lognormal variables can also be well approximated by a lognormal distribution.

4) Weibull distribution:

$$f(x) = \frac{\kappa}{\lambda} \left(\frac{x}{\lambda}\right)^{\kappa-1} e^{-(x/\lambda)^\kappa}, \quad x \geq 0 \quad (3.2)$$

where λ is the scale parameter and κ is the shape parameter of the distribution.

5) Rayleigh distribution: For some environments, the Rayleigh distribution is valid even when the resolvable bin-width is very small.

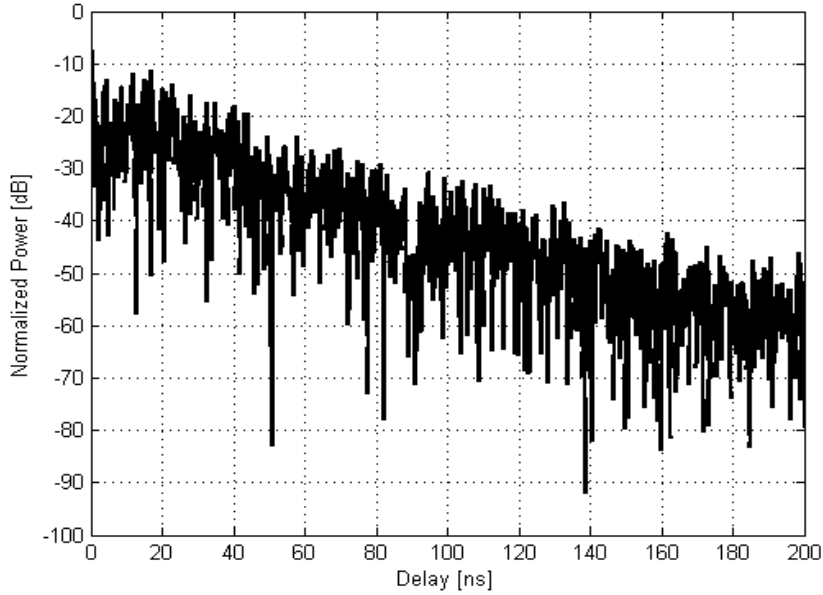


Figure 3.2: Typical the normalized power delay profile of a sample data file for Environment 1

3.4 Small-Scale Fading Distribution by Body

In this section, the small-scale fading statistics in the absence and presence of human bodies in indoor LOS environments are obtained from the measured data and are denoted as the small-scale fading distribution with no body (SFDNB) and with body (SFDB), respectively. The measured data using a VNA is a frequency response of the channel which has both amplitude and phase. The real pass-band inverse Fourier transform is used to transform the measured frequency domain data to the time domain data [32]. The power delay profile (PDP) is extracted from the time domain data and PDPs from 49 local points are gathered. Amplitudes are normalized by the largest amplitude in PDPs of whole 49 local points. Then, the extraction of amplitude for each bin was carried out by collecting a vector of 49 amplitude values with an equivalent delay at 49 local points. Figure 3.2 shows the normalized PDP of a sample data file in the presence of human bodies at the distance of 8m from Tx for Environment 1.

To evaluate the goodness-of-fit for these candidate amplitude distributions, we use the

Kolmogorov-Smirnov ($K - S$) and chi-square (χ^2) hypothesis tests. These two tests compare empirical data and a reference probability distribution. A significance level of 5 % is used in the tests. Due to some limitations in each of these two hypothesis tests [33], both tests are deployed here in order to ensure the reliability of the fitting. Empirical data from bins at specific excess delays were matched to some typical theoretical distributions for amplitude statistics such as Lognormal, Nakagami, and Weibull. Table 3.2 and 3.3 show the passing rate of $K - S$ and χ^2 tests for the above distributions in the absence and presence of human bodies in the environments, respectively. The passing rates in the tables are averaged over delay times. The tables show that the Weibull distribution yields the highest passing rate for both tests in all environments. Therefore, we can assume that the small-scale fading statistics can be modeled by the Weibull distribution.

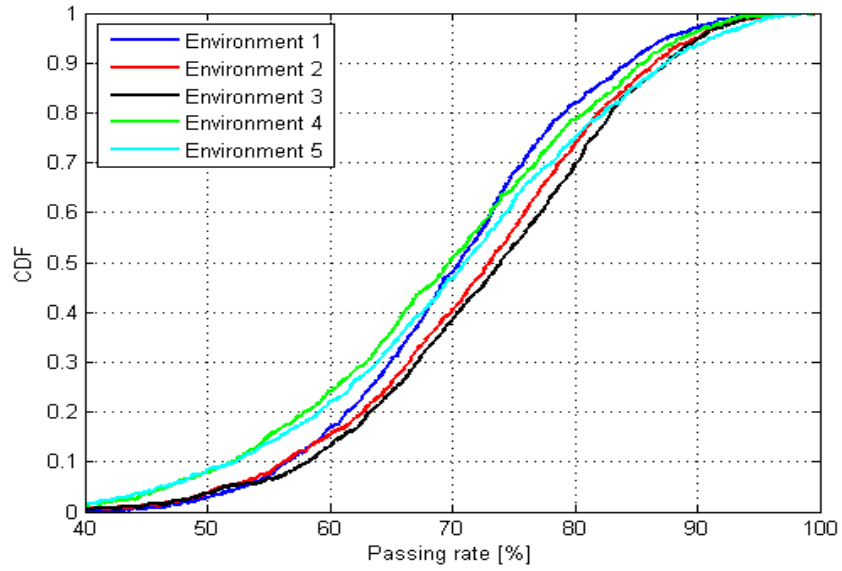
The cumulative distribution functions (CDFs) of passing rates of Weibull distribution for $K - S$ and χ^2 test in the presence of human bodies for all environments are shown in Figure 3.3 (a) and (b), respectively. For the two tests, more than about 80% of bins have more than 65% of passing rates in all environments. Thus, Figure 3.3 shows the small-scale fading amplitude statistics at most of bins are well fitted by Weibull distribution.

Table 3.2: Passing Rate For The Scenarios In The Absence of Human Body

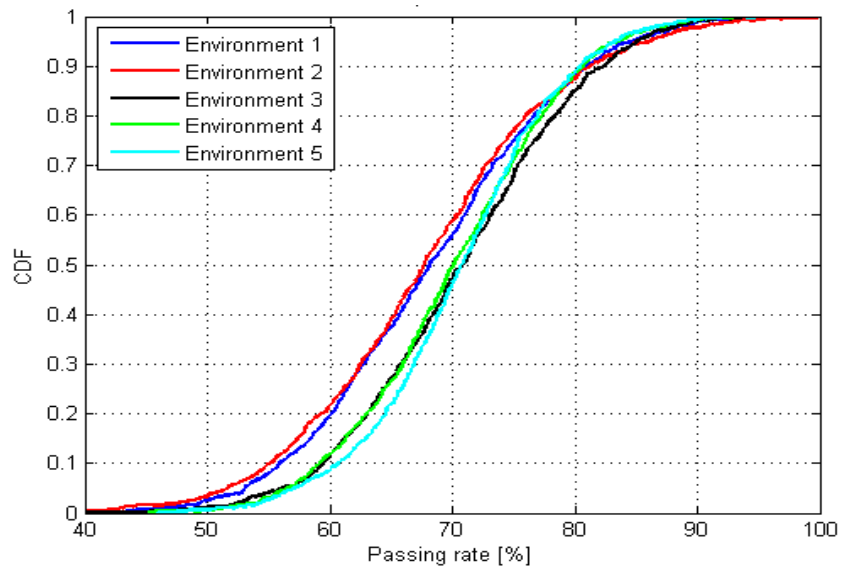
Distribution	Environment 1		Environment 2		Environment 3		Environment 4		Environment 5	
	K-S	χ^2	K-S	χ^2	K-S	χ^2	K-S	χ^2	K-S	χ^2
Lognormal	57.37	3.51	54.39	6.16	61.94	7.38	67.02	12.49	63.55	11.93
Rayleigh	14.97	5.85	12.54	5.53	21.15	9.39	22.49	11.74	24.24	12.87
Nakagami	63.64	61.02	62.93	59.06	64.04	62.26	62.03	56.88	59.52	57.24
Rician	43.71	27.64	13.41	7.76	28.45	24.52	23.33	17.41	24.67	21.31
Weibull	77.23	72.73	78.16	73.89	79.57	76.73	77.54	75.19	75.94	72.42

Table 3.3: Passing Rate For The Scenarios In The Presence of Human Body

Distribution	Environment 1		Environment 2		Environment 3		Environment 4		Environment 5	
	K-S	χ^2	K-S	χ^2	K-S	χ^2	K-S	χ^2	K-S	χ^2
Lognormal	52.89	5.98	57.85	1.76	57.86	8.01	66.75	10.61	63.98	9.85
Rayleigh	18.01	5.53	17.94	4.31	21.85	10.44	21.37	12.87	23.32	16.49
Nakagami	66.63	61.14	67.23	60.89	64.92	61.3	61.41	57.49	61.74	60.03
Rician	46.73	25.36	15.34	8.06	31.32	23.61	26.59	17.38	26.28	19.43
Weibull	70.78	68.82	73.12	67.06	76.92	70.62	69.78	70.05	71.55	72.95

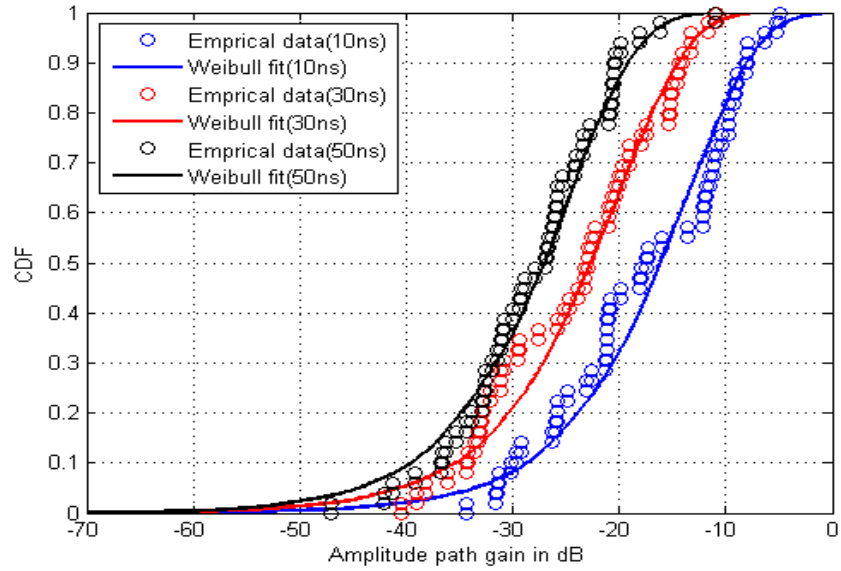


(a)

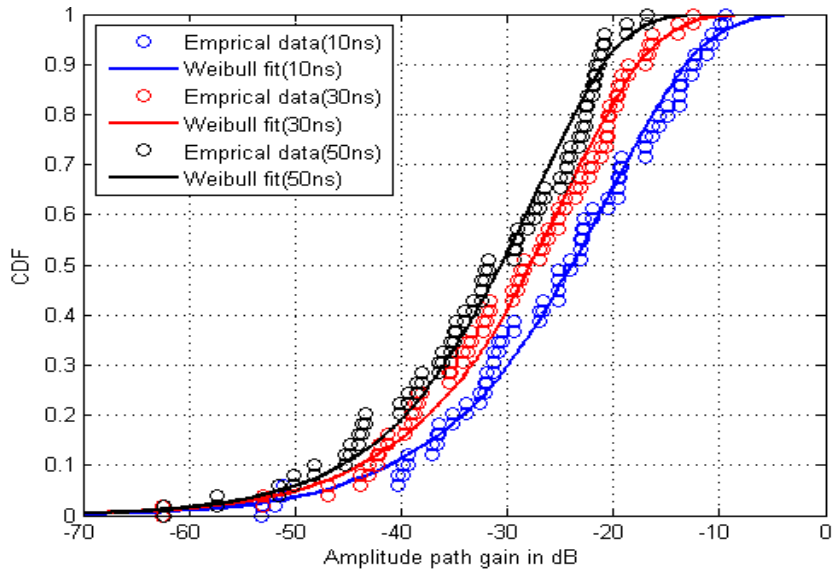


(b)

Figure 3.3: CDFs of passing rate of Weibull distribution for (a) $\kappa - s$ and (b) χ^2 test with the significant level of 5 % in the presence of human bodies



(a)



(b)

Figure 3.4: CDFs of the empirical small-scale fading amplitude fitted with Weibull distribution (a) in the absence of human bodies and (b) in the presence of human bodies for Environment 1 ($D=4\text{m}$)

Figure 3.4 (a) and (b) show CDFs of the empirical small-scale fading amplitude fitted to Weibull distribution at different excess delays at the distance of 4m from Tx in the absence and the presence of human bodies for Environment 1, respectively. At the same position in Environment 1, in Figure 3.4 (a) for when there is nobody in the environment, the amplitudes of small-scale fading are not distributed smaller than -50 dB, but when there are human bodies in the environment, the amplitudes are distributed smaller than -50 dB, which are shown in Figure 3.4 (b). From the figures, the variance range of amplitudes of small-scale fading become larger when there are human bodies in the environment.

From Table 3.2, 3.3, and Figure 3.4, the small-scale fading amplitude statistics are well modeled by Weibull distribution. The Weibull distribution is defined as

$$f(x; \lambda, \kappa) = \frac{\kappa}{\lambda} \left(\frac{x}{\lambda} \right)^{\kappa-1} e^{-(x/\lambda)^\kappa}, \quad x \geq 0 \quad (3.3)$$

where λ is the scale parameter and κ is the shape parameter of the distribution.

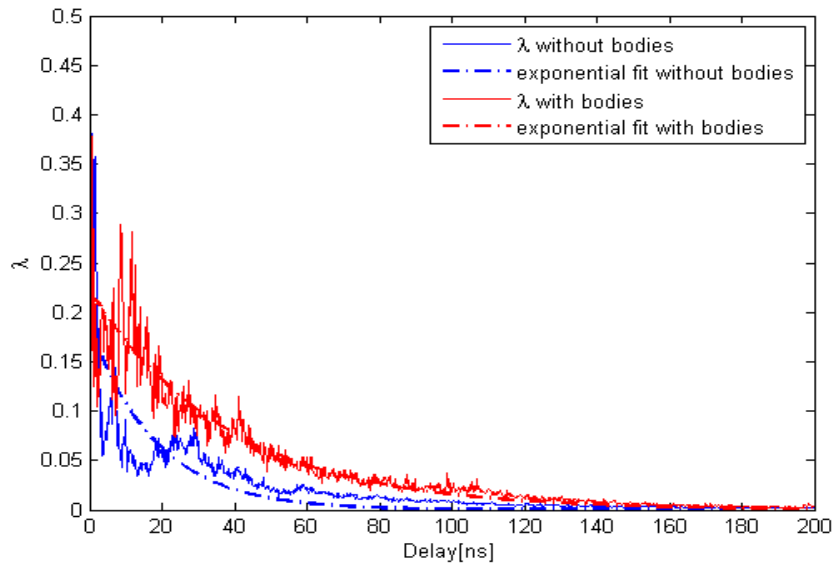
The amplitude and the shape of Weibull distribution depend on two parameters, the scale parameter λ and the shape parameter κ . In this paper, we try to suggest models of two parameters. The λ and κ parameters of the Weibull distribution were extracted from the measurement data using the maximum likelihood estimation (MLE) method for all environments.

We found that the scale parameter of Weibull distribution λ , are well fitted by the exponential function as follow,

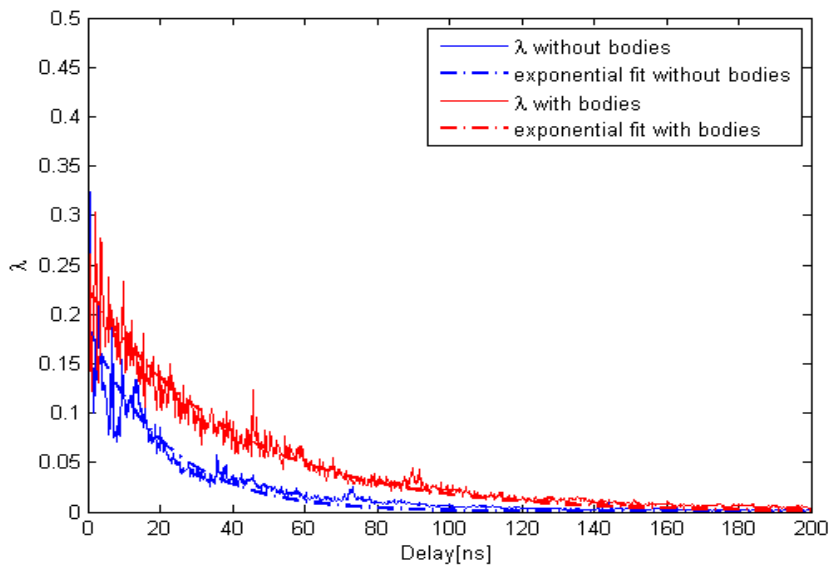
$$f(x; a, b) = a \exp(-bx) \quad (3.4)$$

where a and b are parameters of the exponential function and x is delay times.

Figure 3.5 (a) and (b) describe λ with delay time and its exponential regression model with/without human bodies for Environment 1 and Environment 4, respectively. In the figures, the scale parameter of Weibull distribution λ depends on whether or not human bodies exist in the environment. When there are human bodies in the environment, the scale parameters with delay time are larger than those when nobody exists. For Weibull distribution, the variation range of the distribution increases as the scale parameter λ increases. This result is also shown in Figure 3.4.



(a)



(b)

Figure 3.5: λ with delay time and its regression model fitted with the exponential function for (a) Environment 1(D=4m) and (b) Environment 4 (D=4m)

Table 3.4: The parameters of the exponential fit for λ

	Distance [m]	Exponential fit			
		Without bodies		With bodies	
		a	b	a	b
Environment 1	8	0.218	0.054	0.287	0.028
	4	0.188	0.055	0.222	0.026
	2	0.143	0.051	0.184	0.028
Environment 2	4	0.201	0.049	0.243	0.035
	2	0.128	0.047	0.214	0.031
Environment 3	4	0.197	0.058	0.250	0.026
	2	0.116	0.048	0.211	0.030
Environment 4	8	0.214	0.053	0.285	0.033
	4	0.190	0.048	0.225	0.025
	2	0.144	0.046	0.208	0.030
Environment 5	4	0.189	0.053	0.258	0.034
	2	0.139	0.042	0.186	0.031

Table 3.4 shows the parameters a and b of the exponential regression model of λ by (3.4) in the absence and presence of human bodies. In all environments, a largely depends on the distance, but b does not largely depend on the distance. When there are human bodies in the environments, the parameter of exponential fit a , is larger than one when nobody exists on the same condition. And the parameters b which decide how fast λ decreases with delay times in the presence of human bodies are smaller than those in the absence of bodies. This means that at the same delay time the variation range of small-scale fading amplitudes increases when there are human bodies in the environment.

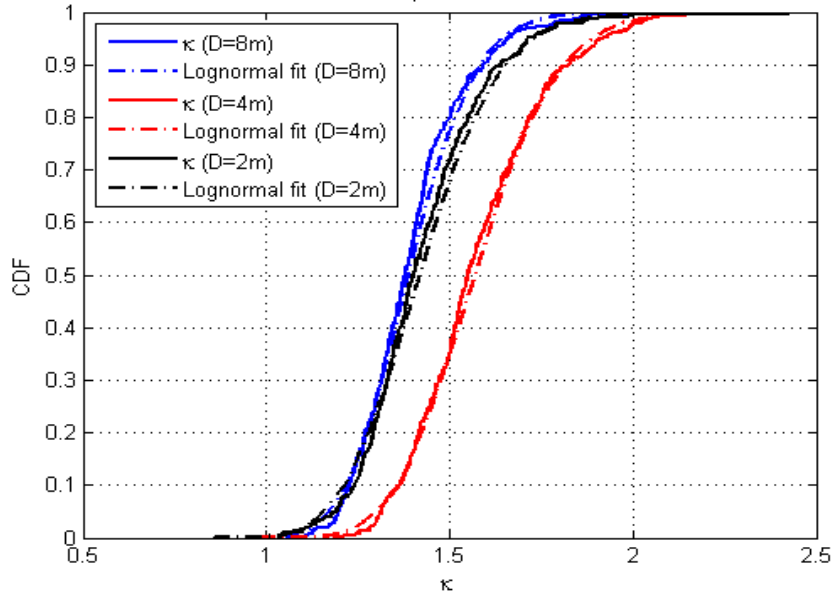


Figure 3.6: CDF of κ and their regression model fitted with Lognormal distribution in the presence of human bodies for Environment 1

As claimed in [23], the shape parameter of Weibull distribution κ are well modeled by the Lognormal distribution as follows

$$f(x; \mu, \sigma) = \frac{1}{x\sigma\sqrt{2\pi}} \exp\left(-\frac{(\ln x - \mu)^2}{2\sigma^2}\right), \quad x > 0 \quad (3.5)$$

Figure 3.6 shows CDFs of κ with different distances and its Lognormal regression models in the presence of human bodies for Environment 1.

Table 3.5 shows the parameters μ and σ of the lognormal regression model of κ by (3.5) in the absence and presence of human bodies. The parameters of Lognormal distribution, μ and σ are related to environments, not to distance. From the table, the parameter, μ in the absence of human bodies is larger than one in the presence of human bodies for the same distance and the same environment, but σ does not depend on the existence of human bodies. Here, the variance of amplitudes of Weibull distribution increases as the shape parameter κ decreases with the fixed scale parameter. This is shown in the parameters μ of Lognormal

Table 3.5: The parameters of the Lognormal fit for κ

	Distance [m]	Lognormal fit			
		Without body		With body	
		μ	σ	μ	σ
Environment 1	8	0.374	0.101	0.327	0.102
	4	0.489	0.111	0.449	0.113
	2	0.395	0.121	0.348	0.122
Environment 2	4	0.419	0.107	0.385	0.108
	2	0.405	0.112	0.378	0.112
Environment 3	4	0.446	0.107	0.421	0.108
	2	0.473	0.111	0.443	0.108
Environment 4	8	0.499	0.112	0.478	0.115
	4	0.484	0.118	0.449	0.118
	2	0.477	0.114	0.443	0.119
Environment 5	4	0.514	0.122	0.496	0.133
	2	0.509	0.113	0.452	0.114

distribution from the table. And also the parameters μ with/without body measured in the office environments are larger than those measured in apartments [23].

3.5 Conclusions

This chapter deals with the small-scale fading distribution in the absence and presence of human bodies in indoor LOS environments. The measurements are carried out in five representative environments having different structures and sizes from each other. From the measurement data, the small-scale fading statistics are best modeled by the Weibull distribution, but the shape and the scale of the distribution depend on two parameters. The chapter makes a model of two parameters. First, the shape parameter of the distribution is modeled by the exponential function with delay time, and the result shows the parameter largely depends on whether or not human bodies exist. The scale parameter of the distribution is modeled by the Lognormal distribution, and μ of the distribution in the presence of human bodies are smaller than those in the absence of human bodies. The results show that the shape parameter of the Weibull distribution increases at the same delay time when human bodies exist in the environment, but the scale parameter decreases. This is because the variance of the small-scale amplitudes increases when there are human bodies exist in the environment. The small-scale fading model in the absence and the presence of human bodies will be helpful to those who want to know the human body effect on UWB channel and validate the results of software simulation of radio-wave propagation in indoor LOS environments

Chapter 4. Performance Analysis of Rake receiver in IR-UWB system

4.1 Introduction

Impulse radio (IR) refers to the generation of a series of impulse like waveforms, each of duration in the hundreds of picoseconds. IR-UWB communicates with baseband pulses of very short duration, typically on the order of a nanosecond, thereby spreading the energy of the radio signal very thinly from near dc to a few gigahertz (GHz). For this reason, IR-UWB system does not require frequency up-conversion and down-conversion. This reduces the complexity and power consumption of transceiver and thus makes IR-UWB suitable for low-complexity and low power wireless sensor network applications.

UWB systems have robustness to multipath fading because of their fine time resolution. This leads to a high diversity order once combined with a Rake receiver. Rake receivers are used in time-hopping impulse radio systems and direct sequence spread spectrum systems for matched filtering of the received signal. The receiver structure consists of a matched filter that is matched to the transmitted waveform that represents one symbol and a tapped delay line that matches the channel impulse response [34]. It is also possible to implement this structure as a number of correlators that are sampled at the delays related to specific number of multipath components; each of those correlators is known as rake finger. Based upon the Rake receivers are three types. The All combining Rake (AC-Rake) receiver captures all most all the energy carried by a very large number of different multipath signals. To reduce the rake complexity, a partial combining (PC-Rake) is used as partial combining of the energy, which combines the first arriving paths out of the available resolved multipath components. Selective combining (SC-Rake) is a suboptimum Rake receiver, which combines the energy selectively carried out by the strongest multipath components.

This chapter deals with BER performance of Rake receiver using the small-scale fading channel model proposed in section 3.3, comparing with previous channel models.

The remainder of the chapter is organized as follows: Section 4.2 presents a UWB Rake receiver structure. In Section 4.3, we briefly introduce existing channel models. Section 4.4 deals with Bit-Error-Rate(BER) performance analysis of IR-UWB system. Finally, Section 4.5 presents the summary and the conclusion.

4.2 UWB Rake Receiver

4.2.1 UWB Rake receiver structure [35]

A UWB rake receiver structure is shown in Figure 4.1.

For a single user system, the continuous transmitted data stream is represented as

$$s(t) = \sum_{k=-\infty}^{k=+\infty} d(k)p(t - kT_s) \quad (4.1)$$

where $d(k)$ are stationary uncorrelated BPSK data and T_s is the symbol duration. The UWB pulse $p(t)$ has duration T_{uwb} .

The channel impulse response is given by

$$h(t) = \sum_{i=0}^M h_i \delta(t - \tau_i) \quad (4.2)$$

M is the total number of paths in the channel.

The received signal first passes through the receiver filter matched to the transmitted pulse and is given by:

$$\begin{aligned} r(t) &= s(t) * h(t) * p(-t) + n(t) * p(-t) \\ &= \sum_{k=-\infty}^{+\infty} d(k) \sum_i h_i m(t - kT_s - \tau_i) + \hat{n}(t) \end{aligned} \quad (4.3)$$

where $p(-t)$ represents the receiver matched filter and $n(t)$ is the Additive White Gaussian Noise (AWGN) with zero mean and variance $N_0/2$. Also, $m(t) = p(t) * p(-t)$ and $\hat{n}(t) = n(t) * p(-t)$.

Combining the channel response with the transmitter pulse shape and the matched filter

$$\hat{h}(t) = p(t) * h(t) * p(-t) = \sum_{i=0}^M h_i m(t - \tau_i) \quad (4.4)$$

The received signal sampled at the l^{th} rake finger in the n^{th} data symbol interval is given by

$$v(nT_s + \tau_l) = \sum_{k=-\infty}^{+\infty} \hat{h}((n-k)T_s + \tau_l) d(k) \quad (4.5)$$

Where τ_l is the delay time corresponding to the l^{th} rake finger and is an integer multiple of T_s .

The rake combiner output at time $t = nT_s$ is

$$y[n] = \sum_{l=1}^L \beta_l v(nT_s + \tau_l) + \sum_{l=1}^L \beta_l \hat{n}(nT_s + \tau_l) \quad (4.6)$$

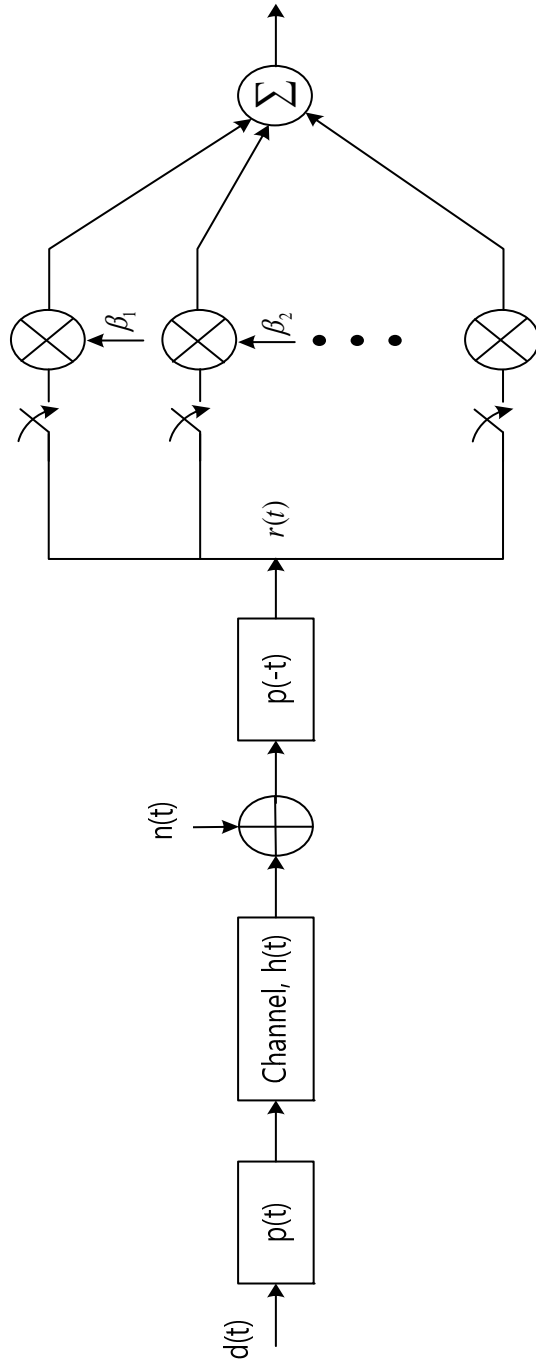
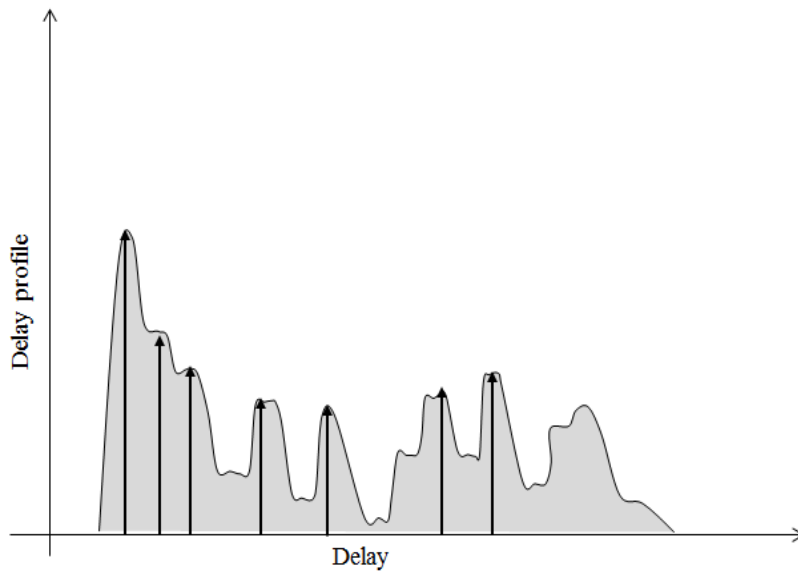


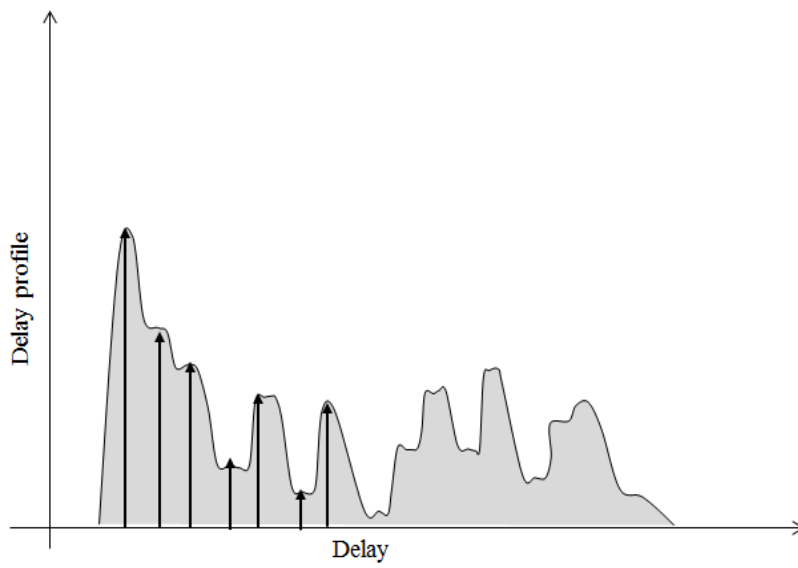
Figure 4.1: A Rake receiver structure

4.2.2 Rake Receiver Type [32]

The received signal energy can be improved in a multipath fading channel by utilizing a diversity technique, such as the rake receiver [32]. Rake receivers combine different signal components that have propagated through the channel by different paths. This can be characterized as a type of time diversity. The combination of different signal components will increase the signal-to-noise ratio (SNR), which will improve link performance. The ideal rake receiver structure captures all of the received signal power by having a number of fingers equal to the number of multipath components. The problem with this approach is the need for an infinite number of rake branches, which also means an infinite number of correlators. Consequently, implementation of the AC-Rake is not possible. A practical rake receiver implementation is a SC-Rake and PC-Rake. The SC-Rake only uses the strongest propagation paths. Figure 4.3 (a) shows the multipath components used by the SC-Rake. The PC-Rake involves combining the first propagation paths. The principle behind this approach is that the first multipath components will typically be the strongest and contain the most of the received signal power. The disadvantage is that the multipath components that the PC-Rake receiver combines are not necessarily the strongest multipath components, so optimum performance will not be achieved. Figure 4.3 (b) shows the multipath components used by the PC-Rake.



(a)



(b)

Figure 4.2: Principle of (a) SC-Rake and (b) PC-Rake receiver [32]

4.3 Channel models

4.3.1 801.15.4a UWB channel model [24]

The CIR defined in the 4a model is a stochastic process, composed of a series of delayed and attenuated multipath components:

$$h(t) = X \sum_{l=0}^{\infty} \sum_{k=1}^{\infty} a_{k,l} \mathcal{D}(t - T_l - t_{k,l}) \quad (4.7)$$

where the cluster arrival and ray arrivals within each cluster are modeled as Poisson processes with arrival rate of Λ and λ , respectively. By definition, the delay of the first cluster is $T_0 = 0$ and the arrival time of other clusters, T_l , has the distribution of Gamma(l, Λ), $l = 1, 2, \dots$. The ray arrival time within a cluster, $t_{k,l}$, has the distribution of Gamma(κ, λ), $\kappa = 1, 2, \dots$. The total excess delay of the k -th ray in the l -th cluster is $\tau_{k,l} = T_l + t_{k,l}$. X represents the log-normal attenuation with zero mean and variance of σ_x^2 . The multipath gain coefficients $a_{k,l}$ are modeled as: $20 \log_{10}(|a_{k,l}|) \sim N(\mu_{k,l}, \sigma_1^2 + \sigma_2^2)$. The average delayed power, $E[|a_{k,l}|^2]$, is represented by double exponential decay:

$$\Omega_{k,l} = E[|a_{k,l}|^2] = \Omega_0 e^{-T_l/\Gamma} e^{-t_{k,l}/\gamma} \quad (4.8)$$

where Ω_0 is the mean power of the first path of the first cluster. The total energy of the multipath components is normalized such that $\sum_{l=0}^{\infty} \sum_{k=0}^{\infty} |a_{k,l}|^2 = 1$. The 3a model follows the Nakagami distribution for the small-scale fading. The distribution of Nakagami is

$$p(x) = \frac{2}{\Gamma(m)} \left(\frac{m}{\Omega} \right)^m x^{2m-1} e^{-(m/\Omega)x^2} \quad (4.9)$$

where $m \geq 1/2$ is the Nakagami m -factor, $\Gamma(m)$ is the gamma function, and Ω is the mean-square value of the amplitude. The m -parameter is modeled as a lognormally distributed random variable, whose logarithm has a mean μ_m and standard deviation σ_m . Both of these can have delay dependence

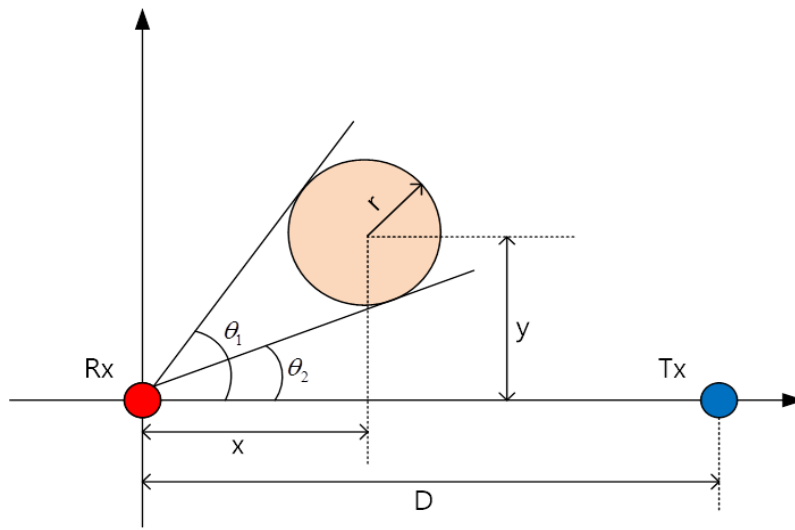
$$\mu_m(\tau) = m_0 - k_m \tau, \quad \sigma_m(\tau) = \hat{m}_0 - \hat{k}_m \tau \quad (4.10)$$

The constant parameters (Λ , λ , Γ , γ , σ_1 , σ_2 , m_0 , and \hat{m}_0) are defined in the 3a standard for four propagation scenarios (CM1~CM4). The parameters of CM3 are used throughout to consider scenarios in indoor office environment with the LOS path between the UWB transceivers.

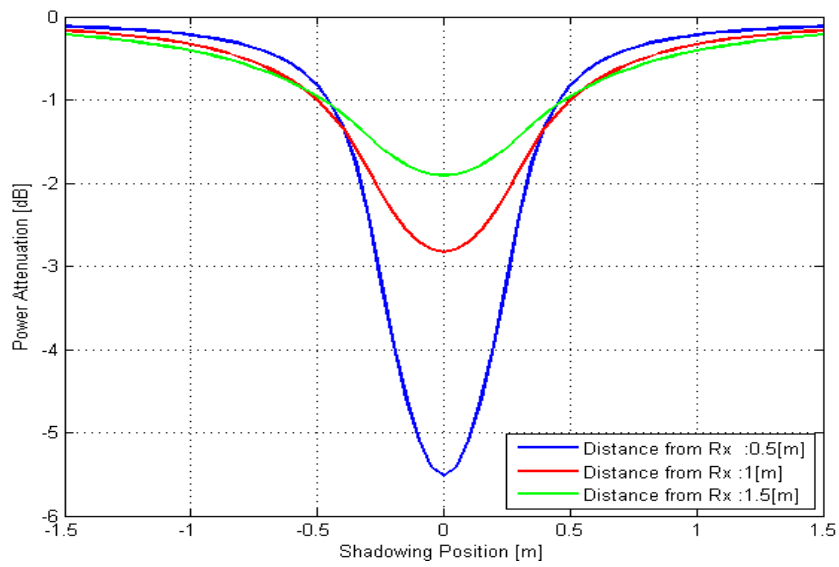
4.3.2 People Shadowing Effect on UWB Channels

In [19], people shadowing effect (PSE) on UWB channels is considered. The paper proposed the PSE model when a person moves along a straight line perpendicular to the LOS path. The PSE model provides a suitable way to determine the shadowing term X instead of using an independent log-normal distributed random variable.

Figure 4.3 (a) shows the blocking angular range with a position with human body: a single scatterer, normally a person, is moving around the area between UWB transceivers and thus obstructing some significant paths. The body is modeled as a cylinder with radius $r = 30$ cm. The numerical results of PSE when a person is passing through the LOS path along a straight line perpendicular to the LOS path from (0.5, -1.5) to (0.5, 1.5) (the unit is m) is shown in Figure 4.3 (b).



(a)



(b)

Figure 4.3: (a) Computation of blocking angular range and (b) Power attenuation when a person moves along a path perpendicular to LOS

4.4 BER performance analysis

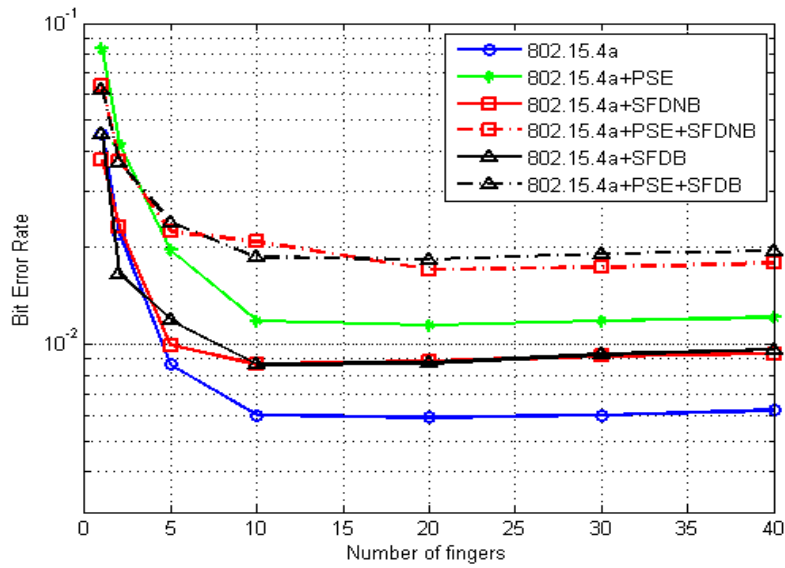
In this section, BER performance of Rake receiver is analyzed for 6 different channel models which are described in Table 4.1. For all channel models, the parameters of 802.15.4a CM 3 channel model which consider scenarios in indoor office environment with the LOS path between the UWB transceiver are used in common [24]. In the table, people shadowing effect (PSE) on UWB channels is considered [19]. This model described the scenario when a person moves along a straight line perpendicular to the LOS path. The PSE model provides a suitable way to determine the shadowing term X instead of using an independent log-normal distributed random variable. During the BER performance simulation in the paper, we assumed the PSE model in which a human body blocked the LOS path to show the worst BER performance. In the table, 802.15.4a and 802.15.4a+PSE channel models use the Nakagami distribution as the small-scale fading model, and the others use the Weibull distribution which is proposed in Section III. When we added the proposed small-scale distribution to 802.15.4a CM3 model, the parameters of Weibull distribution applied to each bin of CM3 CIR, which is to make the amplitude of each bin of CM3 CIR mean value and to follow amplitudes of each bin Weibull distribution. The only difference of between 802.15.4a and 802.15.4a+SFDNB is that small-scale fading distributions of the two models are different, i.e., Nakagami and Weibull distribution, respectively. The two distributions describe different small-scale fading statistics measured in actual environments that have different shape and range of probability density function (PDF) in the statistics. The shape and the range largely depend on the surroundings of Tx and Rx antennas. Under the same mean, the Weibull distribution can cover much smaller variables than the Nakagami distribution. For these reasons, each model uses different distribution that is best fitted to the small-scale fading statistics measured in actual environments. This leads to different shapes and ranges of amplitudes at the same delay time in PDPs. The 802.15.4a+PSE, 802.15.4a+PSE+SFDNB and 802.15.4a+PSE+SFDB channel models include the PSE model as shadowing effect of human bodies described in [19], but the others not. In the table, SFDNB uses the parameters of small-scale fading distribution with no body in Table IV and V, and SFDB uses the parameters with body. In the BER performance

Table 4.1: Main Difference of Channel Models

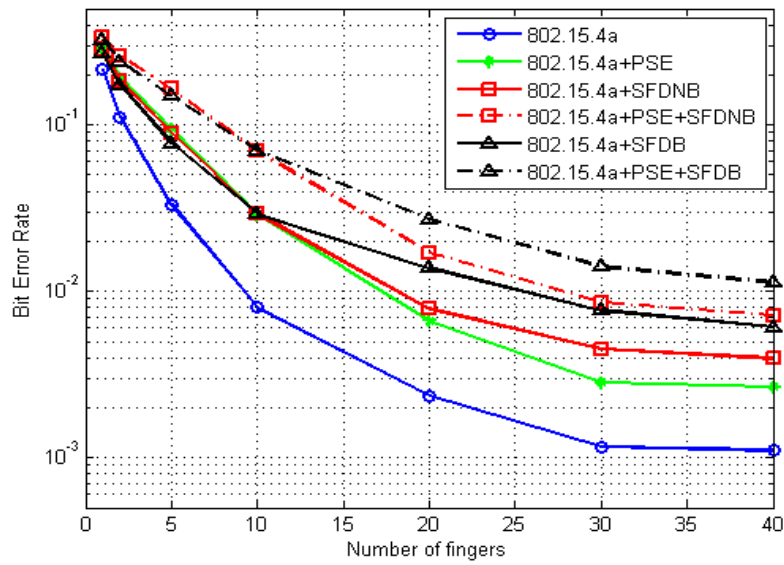
Channel Model	Large scale fading distribution	Small-scale fading distribution
802.15.4a	Lognormal	Nakagami
802.15.4a+PSE	Lognormal, People shadowing effect	Nakagami
802.15.4a+SFDNB	Lognormal	Weibull- without bodies (Table 3.4 and 3.5)
802.15.4a+SFDB	Lognormal	Weibull- with bodies (Table 3.4 and 3.5)
802.15.4a+PSE+ SFDNB	Lognormal, People shadowing effect	Weibull- without bodies (Table 3.4 and 3.5)
802.15.4a+PSE+ SFDB	Lognormal, People shadowing effect	Weibull- with bodies (Table 3.4 and 3.5)

simulation, the channel and transmitted bits are sampled with 0.2174 nsec of the sample duration. The bit duration and bit rate are 21.74 nsec and 46 Mbps, respectively. And the transmitted bits are BPSK modulated.

Figure 4.4 shows the BER of the system with the number of rake fingers for $E_b / N_0 = 10 \text{ dB}$. For SC-Rake receiver in Figure 4.4 (a), the BER performance gets better up to 10 fingers, but the performance does not any better more than 10 fingers. The BER performance for PC-Rake receiver is shown in Figure 4.4 (b). Unlike the result of SC-Rake, the BER performance becomes better as the number of fingers. This is because PC-Rake receiver combines the first arriving paths out of the available resolved multipath components, while SC-Rake receiver combines the instantaneously strongest multipath components. As increasing the number of rake fingers, PC-Rake has a chance to use stronger multipath than multipath earlier arriving.



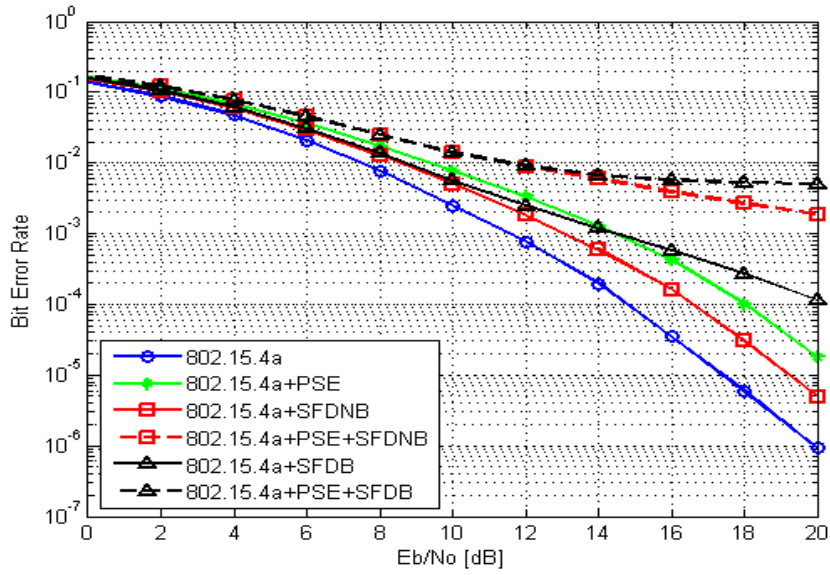
(a)



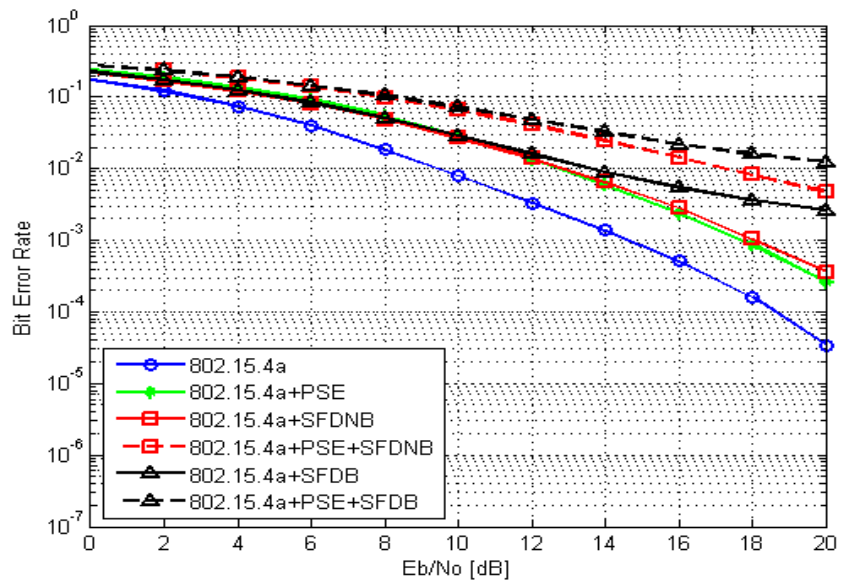
(b)

Figure 4.4: BER with the number of fingers for (a) SC-Rake receiver and (b) PC-Rake receiver (Environment 1)

Figure 4.5 (a) shows the BER performance of a 10-finger SC-Rake receiver. In the figure, the 802.15.4a channel model has the best BER performance with the same E_b/N_0 . The required E_b/N_0 increases when either PSE or SFDB/SFDNB model is included comparing with 802.15.4a model. When both PSE and SFDB/SFDNB model are involved, BER performance of SC-Rake receiver becomes worse. When there are human bodies with the same E_b/N_0 , BER performance gets worse, which is because the channel suffers severe fading by human bodies near to a receiver. These results are shown by comparing 802.15.4a+SFDBNB and 802.15.4a+SFDB or 802.15.4a+PSE+SFDBNB and 802.15.4a+PSE+SFDB in Figure 4.5 (a). At high E_b/N_0 , up to 4 dB is required to meet the same BER performance on the same condition when human bodies exist. In Figure 4.5 (b), the BER performance of a 10-finger PC-Rake receiver is represented. The required E_b/N_0 is up to 4 dB when either PSE or SFDBNB/SFDNB model is included comparing with 802.15.4a model. When both PSE and SFDBNB/SFDNB model are involved, 4 to 12 dB of E_b/N_0 need to meet the same BER performance with 802.15.4a model. As the result of SC-Rake receiver, BER performance of PC-Rake receiver with human bodies is worse than one with nobody. From the figures, SC-Rake receiver has better BER performance than PC-Rake receiver with the same E_b/N_0 for all channel models in Table 4.1, and when there are human bodies around a receiver, BER performance gets worse. In summary, when human bodies exist around a receiver, SFDB model proposed by this paper should be included in the BER performance analysis and more E_b/N_0 required not to deteriorate BER performance.



(a)



(b)

Figure 4.5: BER performance of a 10-finger (a) SC-Rake receiver and (b) PC-Rake receiver (Environment 1)

4.5 Conclusion

This chapter deals with BER performance of Rake receiver using the small-scale fading channel model in section 3.4, comparing with previous channel models. The 802.15.4a channel model which does not consider the human body effect on UWB channel has the best BER performance. The performance becomes worse when either PSE or SFDNB/SFDB model is included in UWB channel. And when both PSE and SFDNB/SFDB model are included, more E_b/N_0 needs to meet the same BER performance on the same condition. And on the same E_b/N_0 , BER performance with human bodies is worse than one with nobody. This result will be helpful to those who want to know the human body effect on BER performance in indoor LOS environments.

Bibliography

- [1] Molisch, A.F., "Ultrawideband propagation channel theory, measurement, and modeling," IEEE Trans. Veh. Tech., vol. 54, no. 5, 2005.
- [2] R. Ganesh and K. Pahlavan, "Effects of traffic and local movements on multipath characteristics of an indoor radio channel", Electron Lett., vol. 26, no. 12, pp. 810-812, Jun. 1990.
- [3] K. I. Ziri-Castro, W. G. Scanlon, and N. E. Evans, "Prediction of variation in MIMO channel capacity for the populated indoor environment using a radar cross-section-based pedestrian model", IEEE Trans. Wireless Commun, vol. 4, no. 3, pp. 1186-1194, May 2005.
- [4] K. I. Ziri-Castro, N. E. Evans and W. G. Scanlon, "Propagation modeling and measurements in a populated indoor environment at 5.2 GHz", AusWireless 2006, 13-16, Mar. 2006, pp. 1-8.
- [5] S. L. Cotton and W. G. Scanlon, "Characterization and modeling of the indoor radio channel at 868 MHz for a mobile bodyworn wireless personal area network", IEEE Antennas Wireless Propag. Lett, vol. 6, pp. 51-55, Dec. 2007.
- [6] T. B. Welch et al, "The effects of the human body on UWB signal propagation in an indoor environment", IEEE J. Sel. Areas Commun., vol. 20, no. 9, pp. 1778-1782, Dec. 2002.
- [7] A. Kara, "Human body shadowing variability in short range indoor radio links at 3-11 GHz", Int. J. Elec, vol. 96, no. 2, pp. 205-211, Feb. 2009.
- [8] J. Karedal, A. J. Johansson, F. Tufvesson and A. F. Molisch, "Shadowing effects in MIMO channels for personal area networks", IEEE VTC 2006 Fall, 25-28 Sep. 2006, pp. 1-5.
- [9] A. Fort, J. Ryckaert, C. Desset, P. De Donecker, P. Wambacq and L. Van Biesen, "Ultra-wideband channel model for communication around the human body", IEEE J. Sel. Areas Commun, vol. 24, no. 4, pp. 927-933, Apr. 2006.
- [10] S. L. Cotton and W. G. Scanlon, "A statistical analysis of indoor multipath fading for a narrowband wireless body area network", IEEE PIMRC06, Sep. 2006, pp. 1-5.
- [11] A. Alomainy, Y. Hao, A. Owaldally, C. G. Parini, Y. I. Nechayev, and C. C. Constantinou and P. S. Hall, "Statistical analysis and performance evaluation for on-body radio propagation

with microstrip patch antennas”, IEEE Trans. Antennas Propag, vol. 55, no. 1, pp. 245-248, Jan. 2007.

[12] A.O. Kaya, L.J. Greenstein, W. Trappe, “Characterizing indoor wireless channels via ray tracing combined with stochastic modeling”, IEEE Trans. Wireless Comm, vol. 8, No. 8, August 2009.

[13] I.Kashiwagi, T.Tagu, T.Imai, “Time-Varying Path-Shadowing Model for Indoor Populated Environments”, IEEE Trans. Veh. Tech, vol. 59, No. 1, Jan. 2010.

[14] S.Chui, D.G.Michelson, “Effect of Human Presence on UWB Radiowave Propagation within the Passenger Cabin of a Midsize Airliner”, IEEE Trans. Antennas Propag, vol. 58, no. 3, pp. 917-926, 2010.

[15] C.G.Spiliotopoulos, A. G.Kanatas, “Path-Loss and Time-Dispersion Parameters of UWB Signals in a Military Airplane”, IEEE Antennas and Wireless Propagation Lett., vol. 8, pp. 790-793, 2009.

[16] S. Obayashi, J. Zander, "A Body-shadowing Model for Indoor Radio Communication Environments," IEEE Trans. Antennas and Propagation, vol. 46, no. 6, June, 1998

[17] M. Ghaddar, L. Talbi, and T.A. Denidni, " Human Body Modeling for Prediction of Effect of People on Indoor Propagation Channel," Electronics letter, vol. 40, no. 25, December, 2004

[18] G. Koutitas,"Multiple Human Effects in Body Area Networks," IEEE Ant and Wireless Propagation Letters, vol. 9, 2010

[19] R. Zhang ; L. Cai, "A Packet-Level Model for UWB Channel with People Shadowing Process Based on Angular Spectrum Analysis," IEEE Trans. Wire. Comm., vol. 8, no. 8, August 2009.

[20] H. Arslan, Z. N. Chen, and M.-G. Di Benedetto, Ultra Wideband Wireless Communications, John Wiley& Sons, 2006.

[21] Q. Li and W. S. Wong, “Measurement and analysis of the indoor UWB channel,” in Proc. IEEE Vehicular Technologies Conf. (VTC 2003-Fall), Orlando, FL, September 2003, pp. 1–5.

[22] D. Cassioli, M. Z. Win, and A. F. Molisch, “The ultra-wide bandwidth indoor channel: from statistical model to simulations,” IEEE J. Select. Areas Commun., vol. 20, no. 6, pp. 1247–1257, August 2002.

- [23] C.-C. Chong, and S. K. Yong, "A Generic Statistical-Based UWB Channel Model for High-Rise Apartments," IEEE Transactions on Antenna and Propagation, Vol. 53, No. 8, August 2005.
- [24] J. Foerster et al., "Channel modeling sub-committee report final," IEEE802.15-02/490, Tech. Rep., Feb. 2003.
- [25]] A. Leon-Garcia, "Random processes," in Probability and Random Processes for Electrical Engineering, 2nd ed. Reading, MA: Addison-Wesley, 1994.
- [26] T.S. Rappaport, Wireless Communications: Principles and Practice, 2nd ed, Englewood Cliffs, NJ: Prentice-Hall, 2002, vol. 58, no. 3, pp. 917-926, 2010.
- [27] C. C. Chong, Y. Kim, and S. S. Lee, "A modified S-V clustering channel model for the UWB indoor residential environment", IEEE VTC, Spring,2005, pp. 58-62.
- [28] J. Keignart, J.-B. Pierrot, N. Daniele, A. Alvarez, M. Lobeira, J. L. Garcia, G.Valera, and R. P. Torres, "Ultra-wideband concepts forAd hoc networks report on UWB basic transmission loss", U.C.A.N., Tech. Rep. IST-2001-32710, Mar. 2003.
- [29] D. Cassioli, W. Ciccognani, and A. Durantini, "D3.1-UWB Channel Model Report", ULTRAWAVES Tech. Rep. IST-2001-35189, Nov. 2003.
- [30] B. Kannan et al., "UWB Channel Characterization in Office Environments",IEEE, Tech. Rep. , Document IEEE 802.15-04-0439-00-004a, 2004.
- [31] J. D. Parsons, The Mobile Radio Propagation Channel, 2nd ed. Mountain View, CA: Pentech, 1992.
- [32] Ian Oppermann, Matti Hamalainen,Jari Iinatti, UWB theory and applications, Wiley, 2004
- [33] NIST/SEMATECH e-Handbook of Statistical Methods, 2005
- [34] A. Rajeswaran, V. S. Somayazulu, and J. R. Foerster, "Rake performance for a pulse based UWB system in a realistic UWB indoor channel," IEEE International Conference on Communications (ICC'03), vol.4, pp.2879-2883, May 2003.
- [35] Archana and Swati Mahajan, " Performance Analysis of Rake Receivers in IR-UWB System," IOSR Journal of Electronics and Communication Engineering (IOSR-JECE), vol. 6, pp23-27,May 2013

초 록

이 논문에는 실내 환경에서 초광대역 (Ultra WideBand) 통신망이 설치된 경우 송신단과 수신단 주변에 위치하는 인체가 해당 통신망의 채널에 미치는 영향에 대한 연구가 나타나 있다. 기존 통신망과 달리 초광대역 통신망은 정보의 대용량 전송을 위해 넓은 주파수 대역을 사용한다. 넓은 주파수 대역을 사용하므로 인접 통신망에 간섭을 일으킬 여지가 있어 초광대역 통신망은 주로 낮은 전력으로 통신을 해야 한다. 저전력을 사용해야 하는 초광대역 통신망은 가시경로 (Line-of-sight, LOS) 또는 비가시경로 (Non-line-of-sight, NLOS) 중 경로 감쇄가 작은 환경에 주로 설치가 된다. 이러한 환경에서는 초광대역 통신망의 채널은 송신단과 수신단 주변 환경에 크게 영향을 받는다. 본 논문에서는 실내 환경에서 채널의 변화를 일으킬 수 있는 송수신단 주변의 여러 요인 중 인체의 영향에 대해서 다루고자 한다.

우선, 가시경로가 항상 확보되는 강의실 환경에서 인체의 밀집도에 따른 초광대역 무선채널의 변화를 모델링 한다. 서로 다른 구조, 크기, 그리고 재질을 갖는 4곳의 강의실에 대해서 측정을 수행하였으며, 각각의 강의실에는 인체의 수를 달리하여 동일한 수신단 위치에서 실험을 반복적으로 수행하였다. 강의실 내의 사람은 정해진 위치에 의자에 앉아 있으며 측정하는 동안 이동하는 사람은 없고 해당 자리에서 필요 시 작은 움직임은 허용하였다. 단위 면적당 위치하는 사람의 수에 따라 대표적인 초광대역 채널 파라미터인 경로 감쇄 모델과 지연분포 파라미터의 변화를 분석하고 인체의 밀집도에 따른 선형적인 채널 파라미터를 제시하였다. 아울러 넓은 주파수 대역을 사용하는 초광대역 통신망의 주파수 상관특성을 구하여 인체의 밀집도에 따라 주파수 상관특성의 변화도 비교한다.

다음으로는 일반 사무실 구조를 갖는 여러 환경에서 수신단 주변에 위치하는 인체에 의해 Small-scale 페이딩의 영향을 보기 위해 같은 환경에서 인체가 존재하지 않을 경우와 존재하는 경우에 대해서 Small-scale 페이딩을 측정하여 각각에 대해서 해당 페이딩을 모델링하였다. Small-scale 페이딩을 얻기 위해 하나의 수신단 주변 좁은 지역내의 49개의 측정 지점에서 측정을 수행하였다. 좁은 지역에서 측정한 49개의 측정 결과를 이용하여 각각의 지연시간에서 Small-scale 페이딩을 구하여 Small-scale

페이딩을 가장 잘 맞는 확률분포를 찾아 해당 확률분포의 파라미터를 모델링하였다. 이 논문의 마지막 부분에서는 사무실 환경에서 인체의 유무에 따라 다르게 모델링된 Small-scale 페이딩을 이용하여 임펄스 라디오 (Impulse Radio, IR) 초광대역 통신망의 성능 분석을 하였다. 임펄스 라디오 초광대역 통신망은 넓은 주파수 대역으로 인해 분해능이 좋아 레이크 (Rake) 수신기를 사용한다. 레이크 수신기는 다중 경로의 수신 정보를 최대한 이용하여 신호 대 잡음비(SNR)를 크게 해주는 효과가 있다. 임펄스 라디오 초광대역 통신망의 성능분석을 함에 있어서 이 논문에서 제시한 초광대역 채널 모델과 기존 표준 채널 모델을 사용하였을 경우 해당 통신망의 성능의 차이를 비교 분석하였다. 아울러 기존 표준 모델에서 포함하지 않은 인체 Shadowing 모델을 소개하고 성능 분석에 포함하여 비교하였다. 성능 분석 결과를 통해 기존 표준 모델에서 고려하지 않은 인체의 영향을 포함하게 된 경우 임펄스 라디오 초광대역 통신망의 성능 열화가 발생하게 되어 이러한 열화를 막기 위해서는 추가적인 신호 대 잡음비를 확보해줘야 한다.

주요어 : 초광대역 채널 모델링, 인체, 임펄스 라디오 초광대역 통신망, Small-scale 페이딩, 레이크 수신기, BER 성능

학번 : 2007-20949